NASA TECHNICAL NOTE

NASA TN D-4239
C. 1

NASA TN D-4239

EFFECTS OF AXIAL GRADIENTS OF VELOCITY AND MAGNETIC FIELD, ELECTRODE STAGGER, AND ION SLIP ON PARAMETERS IN MHD ACCELERATORS

by Frank Hohl

Langley Research Center
Langley Station, Hampton, Va.

NATIONAL AERONAUTICS AND SPACE ADMINISTRATION • WASHINGTON, D. C. • NOVEMBER 1967

NASA TN D-4239

EFFECTS OF AXIAL GRADIENTS OF VELOCITY AND MAGNETIC FIELD, ELECTRODE STAGGER, AND ION SLIP ON PARAMETERS IN MHD ACCELERATORS

By Frank Hohl

Langley Research Center
Langley Station, Hampton, Va.

NATIONAL AERONAUTICS AND SPACE ADMINISTRATION

For sale by the Clearinghouse for Federal Scientific and Technical Information
Springfield, Virginia 22151 – CFSTI price $3.00

EFFECTS OF AXIAL GRADIENTS OF VELOCITY AND MAGNETIC FIELD, ELECTRODE STAGGER, AND ION SLIP ON PARAMETERS IN MHD ACCELERATORS

By Frank Hohl
Langley Research Center

SUMMARY

The distributions of current and potential have been determined for two linear Faraday plasma accelerators that are under investigation at the Langley Research Center. The equations describing the electrical parameters of accelerators were reduced to two dimensions and numerical analysis was used to solve the equations. The internal resistance of the accelerator, the Hall potential gradient, and various other parameters have been calculated as functions of: velocity and magnetic field gradients along the channel axis, ion slip, various amounts of stagger of electrodes, the ratio of electrode width to insulator width, and the Hall parameter $\omega_e\tau_e$. The results are compared with previous theoretical work and with experimentally obtained data.

INTRODUCTION

In the Faraday accelerator, the Hall or electron drift current is reduced by using segmented electrodes which allow an electric Hall field along the channel axis. Since the electric field will be short circuited locally by the finite-length electrodes, strong nonuniformities in the current distribution can be expected near the electrodes. Therefore, a theory describing the electrical properties of an accelerator must use an analysis which is at least two dimensional.

The mathematical formulation of the interaction between the electromagnetic fields and the plasma is given by the generalized Ohm's law which has been derived by Cowling (ref. 1). By using such an Ohm's law, the distribution of current and potential in plasma accelerators and generators has been derived by Hurwitz et al. (ref. 2), Schultz-Grunow and Denzel (ref. 3), Witalis (refs. 4 and 5), Dzung (refs. 6 and 7), and others by means of conformal mappings. Crown (ref. 8) and Celinsky and Fischer (ref. 9) have used numerical methods to solve for the current flux function. Salvat (ref. 10) has used simple physical arguments to investigate the internal potential fall and resistance of magnetohydrodynamic (MHD) generators. In most of these analyses, the effects of ion slip are neglected and in all the analyses, the fluid flow velocity and the applied magnetic field

were assumed not to vary along the channel. Also the effect of shifting anodes with respect to the corresponding cathodes was not sufficiently investigated.

In all accelerators there is a velocity gradient and in one of the accelerators that is being developed at the Langley Research Center (ref. 11) there is a relatively large gradient of the applied magnetic field in the flow direction. With a gradient of either velocity or magnetic field, the current and the electric field are no longer uniform in the channel center. The condition of homogeneous current distribution in the channel center which has been used by various authors (refs. 2, 4, and 5) who investigated the problem by means of conformal mappings no longer applies. Instead of uniformity in the channel center, some of the authors (refs. 3 and 12) assumed rectilinear current dividing lines oblique to the channel axis. This condition also is violated when the aforementioned magnetic field and velocity gradients are present. Of course, in addition to the non-homogeneity in the channel center, there are more serious problems if a solution is attempted by means of a conformal mapping in the presence of axial velocity and magnetic field gradients, since a Poisson equation must be solved instead of a Laplace equation.

The purpose of the present analysis is to investigate the effect on the current and potential distribution of velocity and magnetic field gradients, of ion slip, of various amounts of stagger of the electrodes, of the ratio of electrode width to insulator width, and of the Hall parameter $\omega_e \tau_e$.

In the present analysis the boundary layers and the sheaths near the electrodes and insulators were neglected. Also the fluid properties are assumed not to vary across the channel. Kerrebrock (ref. 13) has investigated the effects of variations of the fluid properties across the channel. The magnetic Reynolds number is assumed to be small compared with unity and thus the induced magnetic field can be neglected.

SYMBOLS

The mksA system of units is used herein.

a	quantity defined by equation (17)
b	quantity defined by equation (18)
B	magnetic induction
C	function defined by equation (42)
d	electrode width

e	insulator width
E	electric field
f	function defined by equation (23)
g	function defined by equation (22)
h	function defined by equation (24)
$\hat{i}, \hat{j}, \hat{k}$	unit vectors in the x-, y-, and z-direction, respectively
j	electric current density
l	accelerator channel height
m,n	summation indices
q	proton charge
s	electrode plus insulator width
U	magnitude of velocity
V	velocity
x,y,z	distance along X-, Y-, and Z-axes, respectively
β	Hall parameter
γ	current flux function
ϵ	efficiency
ν	convergence parameter
ρ	quantity defined by equation (29)
σ_o	scalar conductivity

τ	mean collision time
φ	electric potential
φ_a	constant defined by equation (29)
φ_h	function defined by equation (29)
ω	cyclotron frequency, $\frac{qB}{m}$

Subscripts:

e	electron
eff	effective
i	ion
m,n	summation indices
o	initial
T	total
x,y,z	x-, y-, and z-components

Mathematical notations:

$\rightarrow$	vector
$\hat{}$	unit vector
$\lvert\ \rvert$	absolute value

BASIC EQUATIONS AND ANALYSIS

For the case of negligible electron pressure gradients and no time dependence, the generalized Ohm's law is given by (refs. 1 and 12)

$$\vec{j} = \sigma_o\left(\vec{E} + \vec{V} \times \vec{B}\right) - \frac{\omega_e\tau_e}{B}\,\vec{j} \times \vec{B} + \frac{\omega_i\tau_i\omega_e\tau_e}{B^2}\left(\vec{j} \times \vec{B}\right) \times \vec{B} \tag{1}$$

The last term in equation (1) is the ion slip term and it appears because the ions do not transfer their field-acquired momentum with complete efficiency to the neutral particles. Thus, ion slippage generates heat due to friction and causes, in effect, a decrease in the electrical conductivity of the plasma.

The geometry of the accelerator channel is shown in figure 1. The flow velocity of the medium is in the positive x-direction and the applied magnetic field points in the negative z-direction; that is, $\vec{V} = U\hat{i}$ and $\vec{B} = B\hat{k}$ where $B = B_z$. It is also assumed that all quantities vary only in the x,y plane or $\frac{\partial}{\partial z} = 0$. Thus, equation (1) can be written in component form as

$$j_x = \sigma_o E_x - \beta_e j_y - \beta_e\beta_i j_x \tag{2}$$

$$j_y = \sigma_o\left(E_y - UB\right) + \beta_e j_x - \beta_e\beta_i j_y \tag{3}$$

where $\beta_e = \omega_e\tau_e$ and $\beta_i = \omega_i\tau_i$ and σ_o is assumed to be constant not only in the axial direction but also across the channel.

Equations (2) and (3) can be solved for j_x and j_y to give

$$j_x = \frac{\sigma_o}{\beta_e^2 + \left(1 + \beta_e\beta_i\right)^2}\left[E_x\left(1 + \beta_e\beta_i\right) - \left(E_y - UB\right)\beta_e\right] \tag{4}$$

$$j_y = \frac{\sigma_o}{\beta_e^2 + \left(1 + \beta_e\beta_i\right)^2}\left[E_x\beta_e + \left(E_y - UB\right)\left(1 + \beta_e\beta_i\right)\right] \tag{5}$$

Since the effect of flow velocity gradients and magnetic field gradients along the channel is to be investigated, the x-dependence of U and B must be included. Also, since β_e and β_i are proportional to B, these quantities will also vary with x. As has been discussed by Yeh and Sutton (ref. 14), a variation of the velocity across the channel does not affect the distribution of $\vec{E}$ and $\vec{j}$ (except for a constant factor).

The problem under investigation is time independent so that the Maxwell equation for the conservation of charge becomes

$$\nabla \cdot \vec{j} = \frac{\partial j_x}{\partial x} + \frac{\partial j_y}{\partial y} = 0 \tag{6}$$

Let

$$\sigma_{eff}(x) = \frac{\sigma_o}{\beta_e^2 + \left(1 + \beta_e\beta_i\right)^2} \tag{7}$$

then by using equations (4) and (5) for j_x and j_y, respectively, equation (6) becomes

$$\left[E_x(1 + \beta_e\beta_i) - (E_y - UB)\beta_e\right]\frac{\partial}{\partial x}(\ln \sigma_{eff}) + \left(\frac{\partial E_x}{\partial x} + \frac{\partial E_y}{\partial y}\right)(1 + \beta_e\beta_i)$$

$$+ E_x \frac{\partial}{\partial x}\beta_e\beta_i - E_y \frac{\partial \beta_e}{\partial x} + \frac{\partial(UB\beta_e)}{\partial x} = 0 \tag{8}$$

where β_e, β_i, and σ_{eff} are assumed not to vary in the y-direction. In obtaining equation (8), the Maxwell equation $\nabla \times \vec{E} = 0$ was used to eliminate two terms. A potential $\varphi(x,y)$ is now introduced such that

$$\vec{E} = -\nabla\varphi \tag{9}$$

Equation (8) then takes the form

$$\left(\frac{\partial^2\varphi}{\partial x^2} + \frac{\partial^2\varphi}{\partial y^2}\right)(1 + \beta_e\beta_i) + \frac{\partial\varphi}{\partial x}\frac{\partial(\beta_e\beta_i)}{\partial x} - \frac{\partial\varphi}{\partial y}\frac{\partial\beta_e}{\partial x} - \frac{\partial}{\partial x}(UB\beta_e)$$

$$+ \left[(1 + \beta_e\beta_i)\frac{\partial\varphi}{\partial x} - \beta_e\left(\frac{\partial\varphi}{\partial y} + UB\right)\right]\frac{\partial}{\partial x}\ln \sigma_{eff} = 0 \tag{10}$$

For the case of constant U, B, and β, equation (10) becomes the Laplace equation

$$\frac{\partial^2\varphi}{\partial x^2} + \frac{\partial^2\varphi}{\partial y^2} = 0 \tag{11}$$

All the previous analyses of the potential and current distribution in MHD accelerators did not solve the equation for the electric potential but solved an equation for the current flux function $\gamma(x,y)$. Thus if E_x and E_y are eliminated from equations (2) and (3) by the use of $\nabla \times \vec{E} = 0$, the following equation results:

$$\left(\frac{\partial j_y}{\partial x} - \frac{\partial j_x}{\partial y}\right)(1 + \beta_e\beta_i) + j_y \frac{\partial}{\partial x}(\beta_e\beta_i) - j_x \frac{\partial\beta_e}{\partial x} + \sigma_o \frac{\partial}{\partial x}(UB) = 0 \tag{12}$$

where $\nabla \cdot \vec{j} = 0$ has been used to eliminate two terms. Defining the current flux function γ by

$$j_x = \frac{\partial\gamma}{\partial y} \tag{13}$$

and

$$j_y = -\frac{\partial\gamma}{\partial x} \tag{14}$$

equation (12) can be written as

$$\left(\frac{\partial^2\gamma}{\partial x^2}+\frac{\partial^2\gamma}{\partial y^2}\right)\left(1+\beta_e\beta_i\right)+\frac{\partial\gamma}{\partial x}\frac{\partial}{\partial x}\left(\beta_e\beta_i\right)+\frac{\partial\gamma}{\partial y}\frac{\partial\beta_e}{\partial x}-\sigma_o\frac{\partial(UB)}{\partial x}=0 \tag{15}$$

where β_e and β_i were assumed to be functions only of x. As before, if U, B, and β are constant, the equation to be solved reduces to the Laplace equation

$$\frac{\partial^2\gamma}{\partial x^2}+\frac{\partial^2\gamma}{\partial y^2}=0 \tag{16}$$

In the present analysis equation (10) was used to obtain the potential φ. Once φ is known, $\vec{j}$ and $\vec{E}$ can be obtained by using equations (2), (3), and (9).

The equations for the potential distribution in the accelerator are solved for a small section of the accelerator at a time. Therefore, any variation of U and B along the accelerator channel can be approximated by expanding these quantities in a Taylor series and keeping only terms linear in x. Thus, the variation of U and B becomes

$$U=U_o(1+ax) \tag{17}$$

and

$$B=B_o(1+bx) \tag{18}$$

Since ω_i and ω_e are proportional to B, these two quantities vary as $1+bx$. Equations (4) and (5) can then be written as

$$j_x=\sigma_o\frac{E_x\left[1+\beta_e\beta_i(1+bx)^2\right]-E_y\beta_e(1+bx)+U_oB_o\beta_e(1+ax)(1+bx)^2}{\left[1+\beta_e\beta_i(1+bx)^2\right]^2+\left[\beta_e(1+bx)\right]^2} \tag{19}$$

and

$$j_y=\sigma_o\frac{E_x\beta_e(1+bx)+E_y\left[1+\beta_e\beta_i(1+bx)^2\right]-U_oB_o\left[1+\beta_e\beta_i(1+bx)^2\right](1+ax)(1+bx)}{\left[1+\beta_e\beta_i(1+bx)^2\right]^2+\left[\beta_e(1+bx)\right]^2} \tag{20}$$

where β_e and β_i are the values corresponding to B_o. Equation (10) then takes the form

$$\frac{\partial^2\varphi}{\partial x^2}+\frac{\partial^2\varphi}{\partial y^2}+g(x)\frac{\partial\varphi}{\partial x}+f(x)\frac{\partial\varphi}{\partial y}=h(x) \tag{21}$$

where

$$g(x) = \frac{2b\beta_e\beta_i(1 + bx)}{1 + \beta_e\beta_i(1 + bx)^2} - \frac{2b(1 + bx)\left\{2\beta_e\beta_i\left[1 + \beta_e\beta_i(1 + bx)^2\right] + \beta_e^2\right\}}{\left[1 + \beta_e\beta_i(1 + bx)^2\right]^2 + \beta_e^2(1 + bx)^2} \tag{22}$$

$$f(x) = \frac{b\beta_e}{1 + \beta_e\beta_i(1 + bx)^2}\left(\frac{2(1 + bx)\left\{2\beta_e\beta_i\left[1 + \beta_e\beta_i(1 + bx)^2\right] + \beta_e^2\right\}}{\left[1 + \beta_e\beta_i(1 + bx)^2\right]^2 + \beta_e^2(1 + bx)^2} - 1\right) \tag{23}$$

and

$$h(x) = \frac{U_oB_o\beta_e(1 + bx)}{1 + \beta_e\beta_i(1 + bx)^2}\left(a + 3abx + 2b - \frac{2b(1 + ax)(1 + bx)^2\left\{2\beta_e\beta_i\left[1 + \beta_e\beta_i(1 + bx)^2\right] + \beta_e^2\right\}}{\left[1 + \beta_e\beta_i(1 + bx)^2\right]^2 + \beta_e^2(1 + bx)^2}\right) \tag{24}$$

To obtain the potential distribution in the channel, equation (21) was solved numerically with the appropriate boundary conditions. At the surface of the conducting electrodes, the potential gradient is taken to be zero; thus,

$$E_x = 0$$

or

$$\varphi = \text{Constant} \tag{25}$$

over the electrode surface. From equations (4) and (5), one then finds that

$$\frac{j_x}{j_y} = \frac{-\beta_e(1 + bx)}{1 + \beta_e\beta_i(1 + bx)^2} \tag{26}$$

over the electrode surface. The current into an insulator is zero; thus

$$j_y = 0$$

or

$$\frac{\beta_e(1 + bx)}{1 + \beta_e\beta_i(1 + bx)^2}\frac{\partial\varphi}{\partial x} + \frac{\partial\varphi}{\partial y} + U_oB_o(1 + ax)(1 + bx) = 0 \tag{27}$$

over the surface of an insulator. One also finds that

$$\frac{E_x}{E_y - UB} = \frac{-\beta_e(1 + bx)}{1 + \beta_e\beta_i(1 + bx)^2} \tag{28}$$

over the insulator surface.

In the present analysis the calculations are performed for the case where each pair of electrodes has a separate power supply. The cathode and corresponding anode can be shifted any amount along the channel but the current out of one electrode equals the current into the other electrode of the pair. This additional boundary condition is then used to fix the potential along the two remaining boundaries as indicated in figure 2 by means of an iterative method. For example, if $a = b = 0$, then the velocity and magnetic field gradients along the channel are zero and $\varphi(x,y) - \varphi(x - 2s,y)$ is a constant, where s equals the sum of the length of one insulator plus one electrode. A section of the generator of length $2s$ was chosen for all the numerical solutions of equation (21). If a or b is not equal to zero then $\varphi(x - 2s,y) - \varphi(x,y) = \varphi_h(y)$. The expression for $\varphi_h(y)$ that was used in most of the calculations is of the form

$$\varphi_h(y) = \varphi_a + \rho y \tag{29}$$

where φ_a and ρ are constants that must be chosen to satisfy the boundary conditions.

It is of interest to determine the fraction of the power input that is used to accelerate the fluid. Let ϵ be the ratio of the work done per unit time by the Lorentz force in the flow direction to the power input; thus,

$$\epsilon = \frac{\iint \vec{V} \cdot \left(\vec{j} \times \vec{B}\right) dx\, dy}{\iint \vec{j} \cdot \vec{E}\, dx\, dy} \tag{30}$$

where ϵ as defined by equation (30) is taken to be the efficiency of the accelerator. For the present problem, this ratio becomes

$$\epsilon = \frac{\iint UBj_y\, dx\, dy}{\iint \left(j_x E_x + j_y E_y\right) dx\, dy} \tag{31}$$

In the numerical calculations, equation (21) was used and only a z-component of the magnetic field was considered. Since it is assumed that $\vec{B}$ is obtained by external excitation, the relation

$$\nabla \times \vec{B} = 0 \tag{32}$$

or

$$\frac{\partial B_z}{\partial x} = \frac{\partial B_x}{\partial z} \tag{33}$$

must be satisfied. For the variation of B_z given in equation (18), one then obtains for B_x the variation

$$B_x = bB_0z \tag{34}$$

where the constant of integration is taken to be zero. The total magnetic field is then given by

$$\vec{B} = \hat{i}bB_0z + \hat{k}B_0(1 + bx) \tag{35}$$

Instead of equations (2) and (3) the following equations for the components of equation (1) are obtained:

$$j_x = \sigma_0 E_x - \frac{\beta_e}{B} B_z j_y + \frac{\beta_e\beta_i}{B^2}\left(B_x B_z j_z - B_z^2 j_x\right) \tag{36}$$

$$j_y = \sigma_0\left(E_y - UB_z\right) - \frac{\beta_e}{B}\left(B_x j_z - B_z j_x\right) - \beta_e\beta_i j_y \tag{37}$$

$$j_z = \sigma_0 E_z + \frac{\beta_e}{B} B_x j_y + \frac{\beta_e\beta_i}{B^2}\left(B_x B_z j_x - B_x^2 j_z\right) \tag{38}$$

The solution of this system of equations is too difficult by a numerical method. To simplify the equations, it can be assumed that $j_z = 0$ since no current can flow through the insulated side walls. From equation (38), such a condition requires a z-component of the electric field given by

$$E_z = -\frac{\beta_e B_x}{B\sigma_0} j_y - \frac{\beta_e\beta_i B_x B_z}{B^2\sigma_0} j_x \tag{39}$$

However, near the electrodes E_z is shorted so that, in general, the z-component of the current density cannot be zero. Thus, in addition to the concentration of current at the upstream edge of the cathode and at the downstream edge of the anode obtained later in the section on results, the x-component of the magnetic field will now cause additional current concentration. Depending on whether b is positive or negative, the current will either concentrate at the center of the electrode edge or at the two ends of the electrode edge. If b or z is small, then the effect of B_x can be assumed to be small and equations (21) to (24) describe the system. In this manner some information about the effect of the axial magnetic field gradient can be obtained even though some simplifying assumptions had to be made. For the case of an axial velocity gradient, no such difficulties exist and the system will remain so that it can be treated as two dimensional.

NUMERICAL SOLUTION

Equation (21) can be written in the following finite difference form:

$$\varphi_{m+1,n}\left[\left(\frac{1}{\Delta x}\right)^2 + \frac{g(x)}{2\Delta x}\right] + \varphi_{m-1,n}\left[\left(\frac{1}{\Delta x}\right)^2 - \frac{g(x)}{2\Delta x}\right] - \varphi_{m,n}\left[\frac{2}{(\Delta x)^2} + \frac{2}{(\Delta y)^2}\right]$$

$$+ \varphi_{m,n+1}\left[\left(\frac{1}{\Delta y}\right)^2 + \frac{f(x)}{2\Delta y}\right] + \varphi_{m,n-1}\left[\left(\frac{1}{\Delta y}\right)^2 - \frac{f(x)}{2\Delta y}\right] = h(x) \tag{40}$$

where Δx and Δy represent the separation of the mesh points used in the numerical solution. The subscripts m,n refer to the mesh points; $n = 1$ represents a line of points along the bottom row of electrodes and insulators; $n = N$ represents the points along the top row of electrodes and insulators of the accelerator channel; $m = 1$ is the leftmost column of mesh points; and m increases with increasing x.

At points along the insulator $j_y = 0$ and equation (27) can be written in finite difference form as

$$2\Delta x\left(\varphi_{m,n+1} - \varphi_{m,n-1}\right) + 2\Delta y C(x)\left(\varphi_{m+1,n} - \varphi_{m-1,n}\right) = -4\Delta x\, \Delta y U_o B_o (1 + ax)(1 + bx) \tag{41}$$

where

$$C(x) = \frac{\beta_e(1 + bx)}{1 + \beta_e\beta_i(1 + bx)^2} \tag{42}$$

Equation (41) is used to eliminate the $\varphi_{m,o}$ or the $\varphi_{m,n+1}$ term which appears in equation (40) whenever any points fall on the insulators. Thus for any points along the bottom insulators, $n = 1$ and

$$\varphi_{m+1,1}\left\{\left(\frac{1}{\Delta x}\right)^2 + \frac{g(x)}{2\Delta x} - \frac{C(x)}{2\Delta x}\left[f(x) - \frac{2}{\Delta y}\right]\right\} + \varphi_{m-1,1}\left\{\left(\frac{1}{\Delta x}\right)^2 - \frac{g(x)}{2\Delta x} + \frac{C(x)}{2\Delta x}\left[f(x) - \frac{2}{\Delta y}\right]\right\}$$

$$- \varphi_{m,1}\left[\frac{2}{(\Delta x)^2} + \frac{2}{(\Delta y)^2}\right] + \varphi_{m,2}\left[\frac{2}{(\Delta y)^2}\right] = h(x) + U_o B_o (1 + ax)(1 + bx)\left[f(x) - \frac{2}{\Delta y}\right] \tag{43}$$

must be satisfied. Also, along the top insulators $n = N$ and the relation

$$\varphi_{m+1,N}\left\{\frac{1}{(\Delta x)^2}+\frac{g(x)}{2\Delta x}-\frac{C(x)}{2\Delta x}\left[f(x)+\frac{2}{\Delta y}\right]\right\}+\varphi_{m-1,N}\left\{\left(\frac{1}{\Delta x}\right)^2-\frac{g(x)}{2\Delta x}+\frac{C(x)}{2\Delta x}\left[f(x)+\frac{2}{\Delta y}\right]\right\}$$

$$-\varphi_{m,N}\left[\frac{2}{(\Delta x)^2}+\frac{2}{(\Delta y)^2}\right]+\varphi_{m,N-1}\left[\frac{2}{(\Delta y)^2}\right]=h(x)+U_oB_o(1+ax)(1+bx)\left[f(x)+\frac{2}{\Delta y}\right] \quad (44)$$

must be satisfied. The boundary condition along the electrodes is $\varphi_{m,1}$ = Constant and $\varphi_{m,N}$ = Constant. Along the two remaining boundaries, the condition given by equation (29)

$$\varphi_{1,n}=\varphi_{M,n}-\varphi_a-\rho y \quad (45)$$

is used. The quantities φ_a and ρ in equation (45) must be chosen so that the current from an anode goes into the corresponding cathode. The correct values of ρ and φ_a are determined by integrating the current density along a line between opposing insulators and satisfying the condition

$$\int j_x\,dy = pI_T \quad (46)$$

where I_T is the total current per unit width of the channel through one electrode and $p = 0, \pm1, \pm2$ depending on the amount of electrode stagger. If U and B are constant, then $\rho = 0$ and only φ_a needs to be determined.

The system of simultaneous equations given by equations (40), (43), and (44) were solved on the IBM 7094 data processing system by an iteration method. The form of equation (40) actually put on the computer is

$$\varphi_{m,n}^{r+1}=\varphi_{m,n}^{r}+\nu(r)\left(\frac{1}{2\left[\left(\frac{1}{\Delta x}\right)^2+\left(\frac{1}{\Delta y}\right)^2\right]}\left\{\varphi_{m+1,n}^{r}\left[\left(\frac{1}{\Delta x}\right)^2+\frac{g(x)}{2\Delta x}\right]+\varphi_{m-1,n}^{r+1}\left[\left(\frac{1}{\Delta x}\right)^2-\frac{g(x)}{2\Delta x}\right]\right.\right.$$

$$\left.\left.+\varphi_{m,n+1}^{r}\left[\left(\frac{1}{\Delta y}\right)^2+\frac{f(x)}{2\Delta y}\right]+\varphi_{m,n-1}^{r+1}\left[\left(\frac{1}{\Delta y}\right)^2-\frac{f(x)}{2\Delta y}\right]-h(x)\right\}-\varphi_{m,n}^{r}\right) \quad (47)$$

Equations (43) and (44) can be done similarly. The superscript r refers to the rth iteration and ν is a convergence factor which was used to speed convergence and could be varied during the solution. For points along the insulators, an equation of the form of equation (47) was initially tried. However, as found by previous workers (refs. 8 and 15), this form of the difference equation caused the numerical solution to blow up. For the points along the insulator, any change in $\varphi_{m,n}^{r+1}$ from the previous iteration was

then divided by $1 + \beta_e$ and fairly rapid convergence was obtained. Another difficulty which was due to the large potential gradients near one edge of the electrodes was encountered. Again this difficulty was primarily for points on the insulator. For the first few mesh points near the electrode edge, there was an oscillation (in space) of the potential such that every other $\varphi_{m,1}$ or $\varphi_{m,N}$ deviated from the "correct" φ. This problem could be reduced but not eliminated by going to a finer mesh size. The difficulty was overcome by checking for the oscillations near the electrode edge during the solution. If the oscillations in φ became appreciable, an averaging of the potential was performed to eliminate the oscillations and the solution was continued until the system converged.

The total power input to the accelerator section was computed by summing

$$\sum_{m=1}^{M} \sum_{n=1}^{N} \left[(j_x)_{m,n} (E_x)_{m,n} + (j_y)_{m,n} (E_y)_{m,n} \right] \Delta x \, \Delta y \tag{48}$$

where j_x and j_y are given by equations (19) and (20) and

$$(E_x)_{m,n} = \frac{1}{2\Delta x} (\varphi_{m-1,n} - \varphi_{m+1,n}) \tag{49}$$

and

$$(E_y)_{m,n} = \frac{1}{2\Delta y} (\varphi_{m,n-1} - \varphi_{m,n+1}) \tag{50}$$

RESULTS

The parameters used for most of the calculations were those that are pertinent for the 1-inch- (2.54-cm) square accelerator presently in operation at the Langley Research Center. These parameters are given in reference 11. To determine the effect of electrode stagger, the following parameters were used: $\sigma_0 = 500$ mho/m, $B_0 = -1.14$ webers/m^2, $\beta_e = -16$, and $U = 400$ m/sec in the midsection of the accelerator channel. The channel is described by the following geometrical parameters: $l = 2.54$ cm, $d = 0.72$ cm, and $e = 0.41$ cm. (See fig. 2.) The applied potential between corresponding electrodes was 200 volts. In order to show the effects of ion slip, the calculations were made for both $\beta_i = 0$ and $\beta_i = -0.04$ with $a = b = 0$. The results are shown in figures 3 to 7. The shift position has been normalized to s, the length of one insulator width plus one electrode width. An increase in the shift position corresponds to moving the anode in the flow direction. In figure 3 the calculated Hall field is plotted as a function of electrode shift position. The results show that the Hall field peaks between the 0 and -1 shift position and that ion slip appreciably reduces the Hall field. Figure 4 shows the effect of electrode stagger on the current per electrode. As

expected, ion slip reduces the current. In contrast to the Hall field, the current peaks at the 0 shift position. Similarly, figure 5 shows that the calculated internal resistance $\frac{\varphi_{applied} + B\bar{U}l}{I_T l}$ between a cathode and the corresponding anode is a minimum at the 0 shift position. The equation for the internal resistance given by Witalis (eq. (42) in ref. 5) was also used to calculate the resistance for zero shift. The results were found to be identical to those given in figure 5 for zero shift. The variation as a function of electrode stagger of the power per unit volume used in accelerating the fluid in the axial direction is shown in figure 6. The acceleration peaks at the zero shift position and at that point ion slip reduces the work done by about 7 percent. Figure 7 shows the calculated effect of electrode stagger on efficiency. It can be seen that the efficiency peaks for zero shift. Ion slip effects reduce the efficiency by only about 2 percent. Thus, the calculations show that shifting the anodes relative to the corresponding cathodes will reduce the efficiency and acceleration. Thus, on the basis of the present calculations, the shifting of the electrodes which has been proposed to increase acceleration (ref. 16) cannot be recommended. Carter et al. (ref. 16) have experimentally investigated the effect of shifting the electrodes. Their results are shown in figures 8 to 10. The experimentally obtained Hall field and current per electrode decreases much more rapidly with shift position than the calculated values. This result is probably due to the effects of the boundary layer near the electrodes and insulators which may cause much stronger variation of the total internal resistance with electrode shift than that calculated. Figure 8 shows a peak in the Hall field between the 0 and -1 shift position which is in agreement with the calculated results. The scatter of the data in figures 9 and 10 is very large and, as a result, it is difficult to compare these experimental results with the calculated values given in figures 4 and 6.

The equipotential and current flux lines in the accelerator section are also of interest. In figure 11 the equipotential lines are shown for the different shift positions for the case with $\beta_i = -0.04$. Figure 12 shows the lines for constant current flux, again for $\beta_i = -0.04$. The difference between the adjacent equipotential lines $\Delta\varphi$ and adjacent current flux lines $\Delta\gamma$ are as given in the figures. The curves were plotted by interpolating between the calculated potential at the different mesh points. Also, since the lines of constant current flux were obtained from the potential by using the approximate formulas for $\vec{E}$ in equations (4) and (5), one cannot expect very high accuracy of the slope of these curves in the region of high current density concentration near the edge of the electrodes. All the equipotential and constant current flux curves were obtained by starting in the lower left-hand corner of the accelerator section where $\gamma = \gamma_0$ and $\varphi = \varphi_0$, and by then finding curves of constant φ and γ given by $\varphi = \varphi_0 \pm n\,\Delta\varphi$ and $\gamma = \gamma_0 \pm n\,\Delta\gamma$ where $n = 1, 2, 3, \ldots$.

An attempt was made to calculate a case which matched the experimentally obtained data given in reference 17. Since the only accurate data available are the average current per electrode and the Hall field, it is not possible to obtain a unique match. For example, for given arbitrary values of β_e and β_i, the applied field E_y can be chosen to give the desired Hall field and σ_o can then be chosen to give the desired current per electrode. It was therefore assumed that $\beta_e = -16$ and $\beta_i = -0.04$ are the correct values for the Hall parameter and the ion slip term, and the applied potential and σ_o were chosen to give the experimentally obtained Hall field and current per electrode as given in reference 17. The magnetic field was -1.14 webers/m^2 and the flow velocity was assumed to be 2000 m/sec at the channel entrance and 6000 m/sec at the exit and to vary linearly in between. Then σ_o was required to be 355 mho/m. In figures 13 to 15 the results of the calculations are compared with the experimental data given in reference 17. Figure 13 shows the measured current per electrode and the current used in the calculations. In figure 14 which shows the calculated and the measured potential between electrodes, the difference between the experimental points and the calculated curve should represent the sheath drop near the electrodes and insulators. The figure indicates that either σ_o increases or the sheath drop decreases near the end of the channel. In figure 15 the calculated electrode potentials and their variation along the accelerator (Hall potential gradient) are compared with the experimental data given in reference 17. The agreement is very good.

The effect of β_e on the electrical parameters of the accelerator has also been calculated. For these calculations β_i was taken to be zero and the voltage applied between an anode and corresponding cathode was 200 V. First the results for the case with B = Constant = -1.14 webers/m^2 and σ = Constant = 500 mho/m are given. Since B and σ are constant, β_e will vary as β = Constant/n where n is the electron density. Figures 16, 17, and 18 show the variation with β_e of the Hall field, the current per electrode, and the efficiency. The variation of the internal resistance is shown in figure 19. Figure 16 shows that for $-\beta_e = 16$ the Hall field is somewhat lower than that shown in figure 15. The reason for this difference is, of course, that the applied potential (or E_y) is lower for the case shown in figure 15. As shown in figure 17 for constant applied voltage, the current per electrode decreases rapidly with increasing Hall parameter. Also shown in figure 17 is the internal resistance as calculated from equation (42) of reference 5. It can be seen that the two methods give identical results except for $-\beta_e$ larger than about 20.

When β_e varies such that $\beta_e = 14B$ and σ_o = Constant = 500, the results are as shown in figures 20 to 23. The efficiency increases almost linearly with $-\beta_e$ but the work done in accelerating the fluid decreases rapidly. For sufficiently large $-\beta_e$, the accelerator would turn into a generator but this transformation occurs only because a constant applied voltage was assumed, and as B increases, so does the

$\vec{U} \times \vec{B} \cdot l$ voltage. For large enough B, this voltage exceeds the applied potential. The internal resistance for this case is the same as that shown in figure 19.

In figure 24 the variation of the internal resistance as a function of the ratio of electrode width to s is shown. The solid line is obtained from the equation for the internal resistance given by Witalis (eq. (42) of ref. 5) and the circles are the values computed by the present numerical method. For the results shown in figure 24, $B = -1.14$, $\sigma_o = 500$, $\beta_i = -0.04$, $s = 0.113$ cm, and $l = 2.54$ cm. Again, there is excellent agreement for the two methods.

In an accelerator the velocity along the channel increases and the quantity a in equation (17) is not zero. In figures 25 and 26 the internal resistance and the efficiency are shown as functions of a. The parameters used are the same as for the previous case with $\beta_e = -16$ and $d = 0.72$ cm. The results shown in figures 25 and 26 show that the internal resistance increases and the efficiency increases with increasing velocity gradients, but both change only slightly over a rather large range of gradient. For $a = 3.33$ (the operating conditions of the 1-inch- (2.54-cm) square accelerator at the Langley Research Center), the equipotential and constant current flux plots are nearly identical to those for $a = 0$. However, for larger a the equipotential lines and constant current flux lines begin to curve, as shown in figure 27. The Hall field along the center line of the accelerator remained constant for increasing a. However, ρ in equation (29) had to be increased to satisfy the boundary conditions. Figure 28 shows ρy_N as a function of a, and indicates how the voltage applied between electrodes must be increased along the accelerator channel.

The effect of magnetic field gradients with the approximations stated earlier has also been investigated. The results are shown in figures 29 to 33. Figure 29 shows that the internal resistance increases slightly with increasing b. As can be seen from figure 30, the efficiency increases as b increases. The change in the equipotential and constant current flux plots is shown in figures 31 and 32. As the magnetic field gradients become large, either negatively or positively, the current density and electric field become increasingly more nonuniform. The effect of b on the applied voltage is indicated in figure 33 which shows ρy_N as a function of b.

For applied magnetic field gradients of the order of the self-induced field, the numerical solution is almost identical to that for a zero magnetic field gradient. This result justifies the neglect of the self-induced field. For increasing velocity and magnetic field gradients, it becomes more difficult to obtain convergence of the numerical solution. The numerical solution could probably be improved by using equation (28) instead of equation (27) as the boundary condition over the insulator surface.

All results presented so far were for the 2.54-cm-square accelerator. Calculations were also performed to determine the effect of electrode stagger for a larger

accelerator with a different ratio of l/s. For this accelerator, l = 6.35 cm, e = 0.476 cm, and d = 0.795 cm. The other parameters used for the calculation were: B = 1.25 webers/m^2, β_e = -10, σ_o = 500 mho/m, U = 7000 m/sec, and a potential difference of 640 volts between corresponding electrodes. The results were found to be very similar to those obtained for the smaller accelerator; consequently, only the effect on the Hall field and the internal resistance are shown (figs. 34 and 35). The internal resistance varies very slowly with shift position.

CONCLUDING REMARKS

The calculated effects of electrode stagger on the electrical parameters of an accelerator were found to be in qualitative agreement with experimental results. It was found that shifting the electrodes will reduce efficiency and acceleration. The more rapid decrease of the parameters found experimentally may be due to the neglect of the variation of the fluid parameters in the vertical (y) direction. The numerically obtained variations of the internal resistance of the accelerator with Hall parameter and ratio of electrode to electrode plus insulator width (d/s) for zero velocity and magnetic field gradients were in agreement with the results obtained by Witalis by means of a conformal method.

With increasing axial velocity and magnetic field gradients, the current density and electric field distribution become increasingly nonuniform in the channel center. However, the variation of the electrical parameters with velocity or magnetic field gradients obtained by the present method indicates that there are no serious detrimental effects on accelerator operation for moderate gradients. Whether problems arise because of additional current concentration due to the appearance of the magnetic induction (B_x) component for axial magnetic field gradients must still be analyzed.

Langley Research Center,
National Aeronautics and Space Administration,
Langley Station, Hampton, Va., May 9, 1967,
129-02-01-01-23.

REFERENCES

1. Cowling, T. G.: Magnetohydrodynamics. Interscience Publ., Inc., 1957.

2. Hurwitz, H., Jr.; Kilb, R. W.; and Sutton, G. W.: Influence of Tensor Conductivity on Current Distribution in a MHD Generator. J. Appl. Phys., vol. 32, no. 2, Feb. 1961, pp. 205-216.

3. Schultz-Grunow, F.; and Denzel, D. L.: Calculation of the Electric Characteristics of an MHD Generator With Finite Electrodes by Conformal Mapping Under Full Consideration of Tensor Conductivity and Velocity Profile. Second International Symposium on MHD Electrical Power Generation (Paris, France), July 1964, pp. 661-676.

4. Witalis, E. A.: Performance of a Segmented Electrode MHD Generator for Various Electrode-Insulator Length Ratios. Plasma Phys., vol. 7, no. 3, May-June 1965, pp. 235-244.

5. Witalis, E. A.: Analysis of Linear MHD Power Generators. Plasma Physics., vol. 7, no. 5, Sept.-Oct. 1965, pp. 455-473.

6. Dzung, L. S.: The MHD Generator in Cross-Connection. Second International Symposium on MHD Electrical Power Generation (Paris, France), July 1964, pp. 601-616.

7. Dzung, L. S.: Favourable Configurations of Segmented Electrodes for MHD Generators. Brown Boveri Review, vol. 53, no. 3, Mar. 1966, pp. 238-250.

8. Crown, J. Conrad: Analysis of Magnetogasdynamic Generators Having Segmented Electrodes and Anisotropic Conductivity. R-1852-2, United Aircraft Corp., Feb. 1961.

9. Celinski, Zdzislaw N.; and Fischer, Fred W.: Effect of Electrode Size in MHD Generators With Segmented Electrodes. AIAA J., vol. 4, no. 3, Mar. 1966, pp. 421-428.

10. Salvat, M.: The Internal Potential Fall in MHD Generators. IPP 3/38, Institut für Plasma Physik, Apr. 1966.

11. Wood, G. P.; Carter, A. F.; Sabol, A. P.; McFarland, D. R.; and Weaver, W. R.: Research on Linear Crossed-Field Steady-Flow D. C. Plasma Accelerators at Langley Research Center, NASA. AGARDograph 84, Sept. 1964, pp. 1-45.

12. Rosa, R. J.: Hall and Ion-Slip Effects in a Nonuniform Gas. Phys. Fluids, vol. 5, no. 9, Sept. 1962, pp. 1081-1090.

13. Kerrebrock, Jack L.: Segmented Electrode Losses in MHD Generators With Non-equilibrium Ionization. AIAA J., vol. 4, no. 11, Nov. 1966, pp. 1938-1947.

14. Yeh, H.; and Sutton, G. W.: Velocity Profiles and Efficiency of MHD Generators With Segmented Electrodes. R61SD150 (AFOSR Document No. 1595), Missile Space Vehicle Dept., Gen. Elec. Co., Sept. 15, 1961.

15. Denison, M. Richard: A Two Dimensional "Weak Interaction Theory" for Crossed Field Accelerators. Res. Note No. 12, Electro-Optical Systems, Inc., Apr. 1963.

16. Carter, A. F.; McFarland, D. R.; Weaver, W. R.; Park, S. K.; and Wood, G. P.: Operating Characteristics, Velocity and Pitot Distribution, and Material Evaluation Tests in the Langley One-Inch-Square Plasma Accelerator. AIAA Paper No. 66-180, Am. Inst. Aeron. Astronaut., Mar. 1966.

17. Carter, A. F.; Wood, G. P.; McFarland, D. R.; and Weaver, W. R.: Research on a One-Inch-Square Linear D-C Plasma Accelerator. AIAA Paper No. 64-699, Am. Inst. Aeron. Astronaut., Aug.-Sept. 1964.

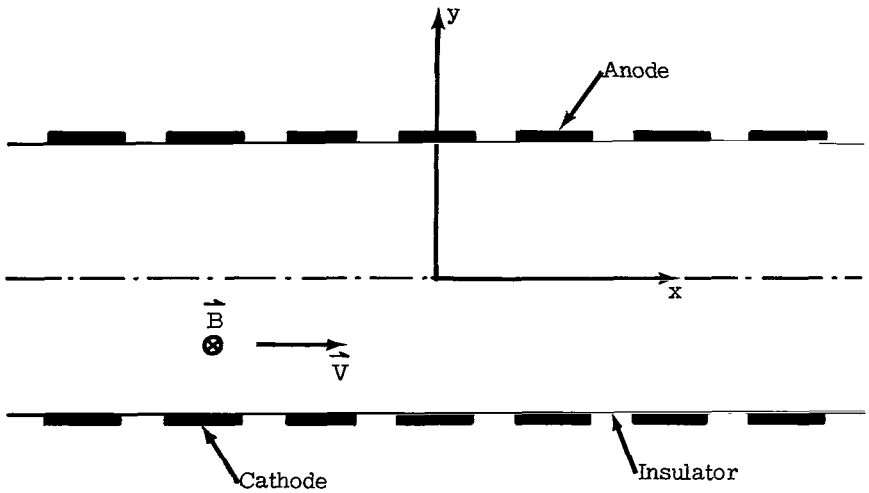

Figure 1.- Geometry of accelerator channel.

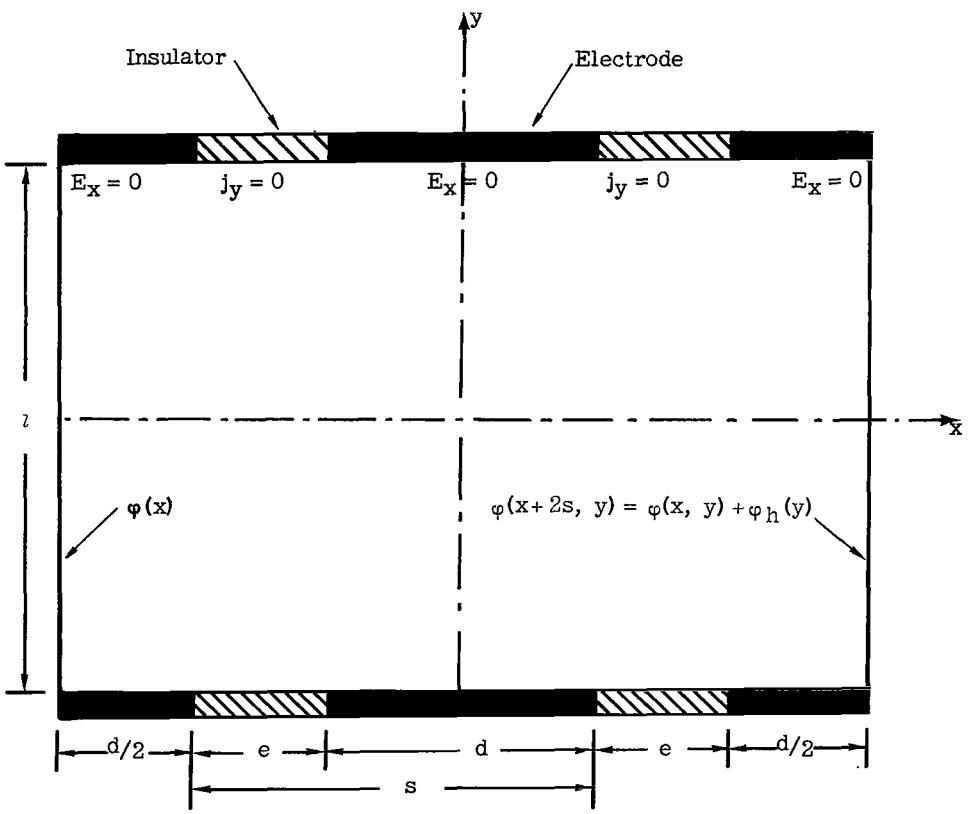

Figure 2.- Geometry and boundary conditions for a section of accelerator channel.

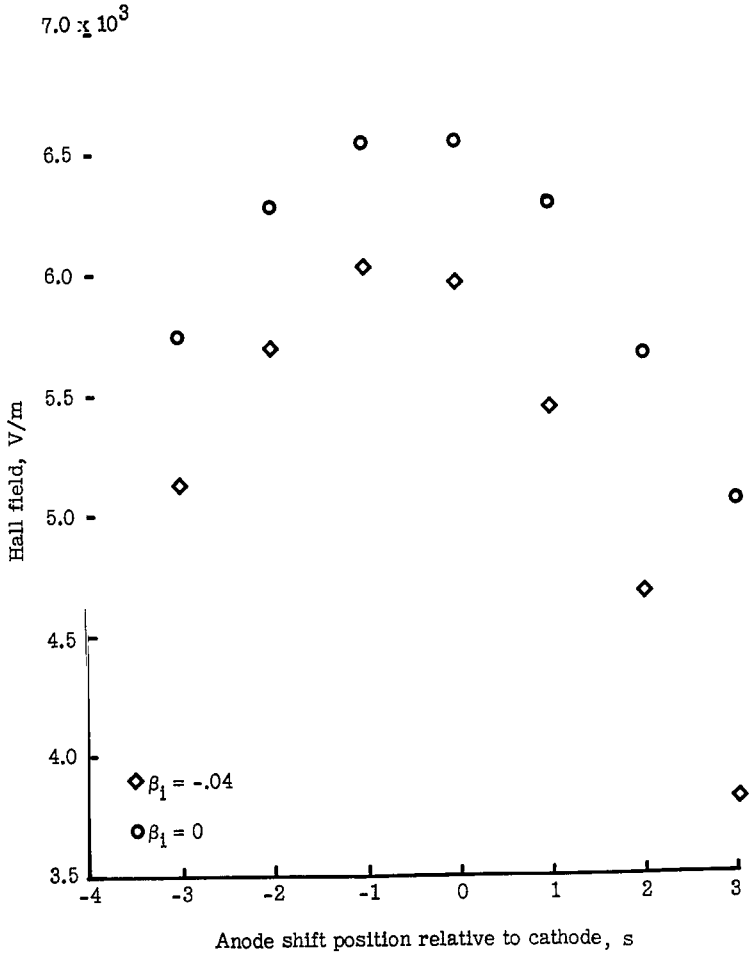

Figure 3.- Effect of electrode stagger on Hall field.

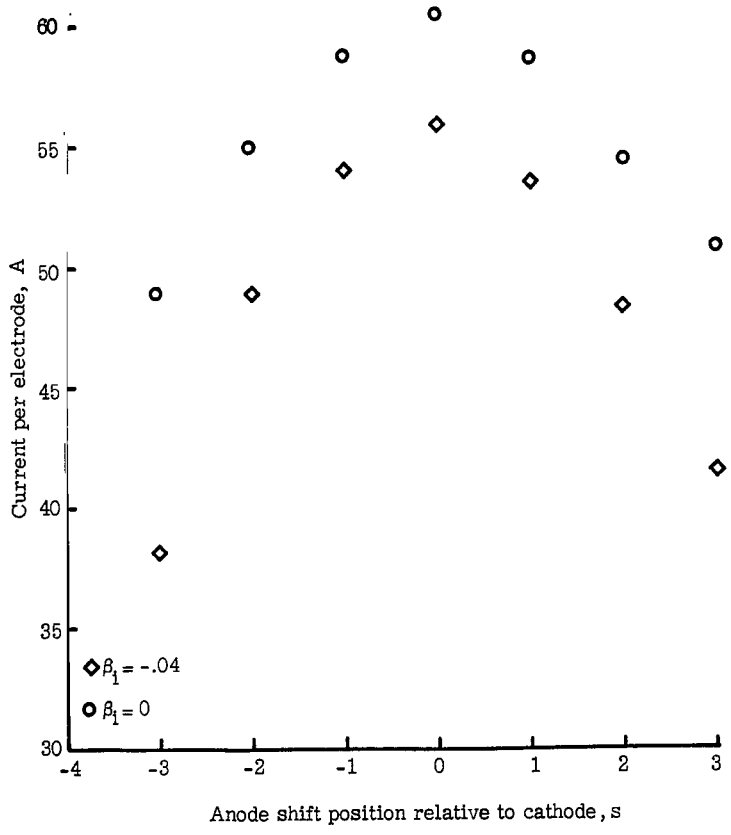

Figure 4.- Effect of electrode stagger on current.

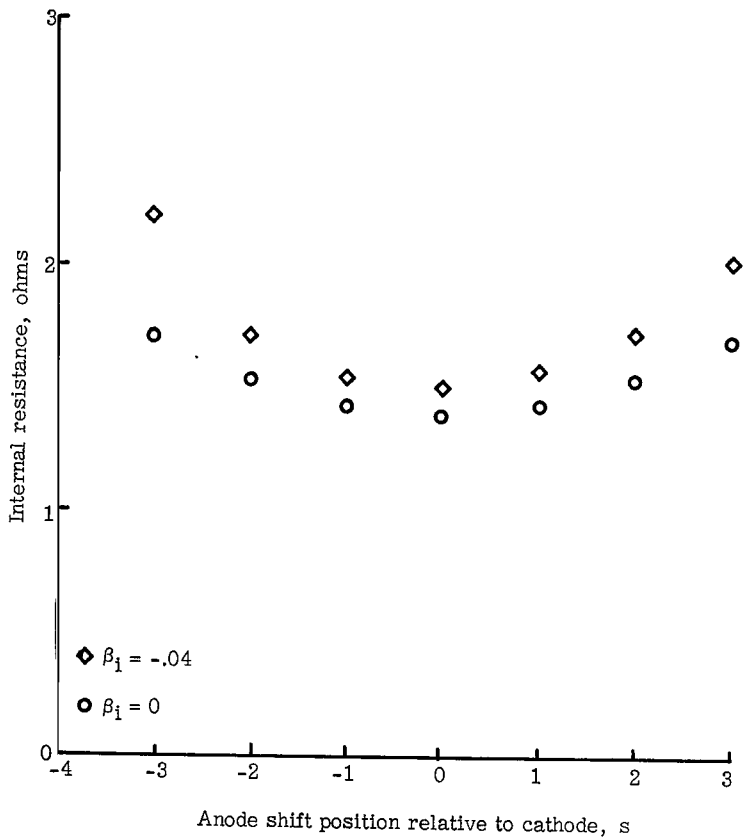

Figure 5.- Effect of electrode stagger on the internal resistance between electrodes.

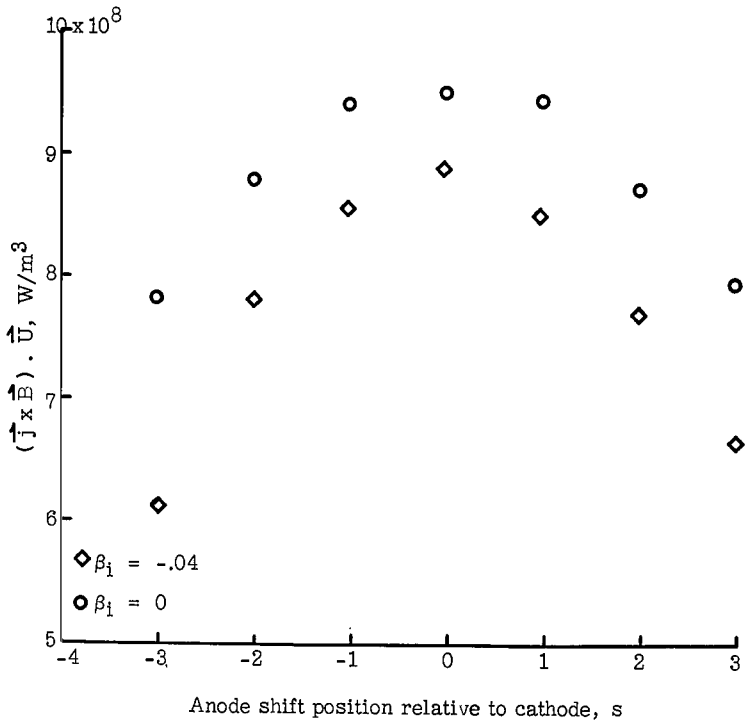

Figure 6.- Effect of electrode stagger on work done to accelerate the flow.

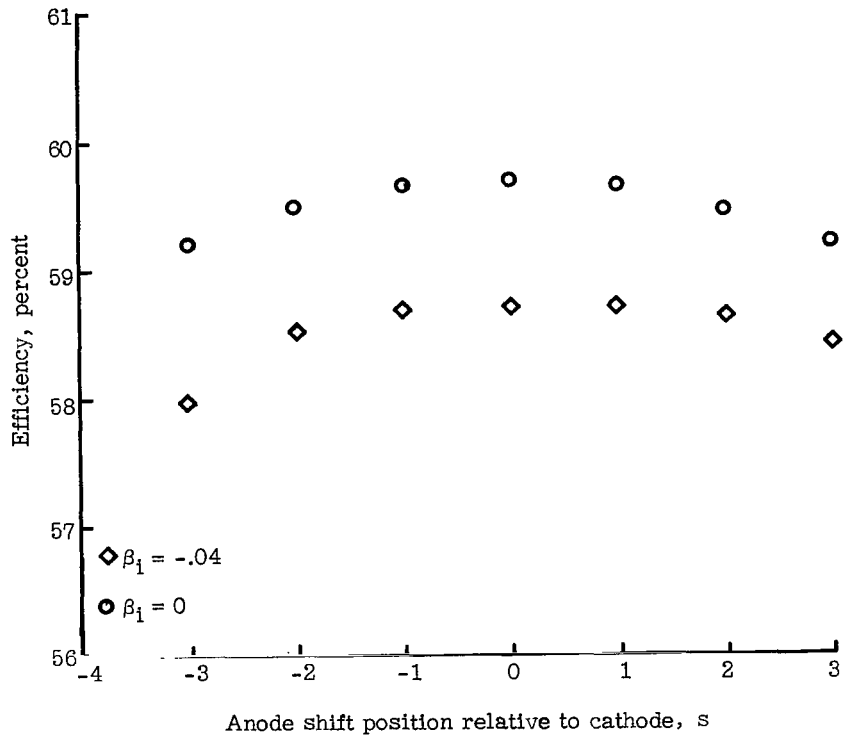

Figure 7.- Effect of electrode stagger on accelerator efficiency.

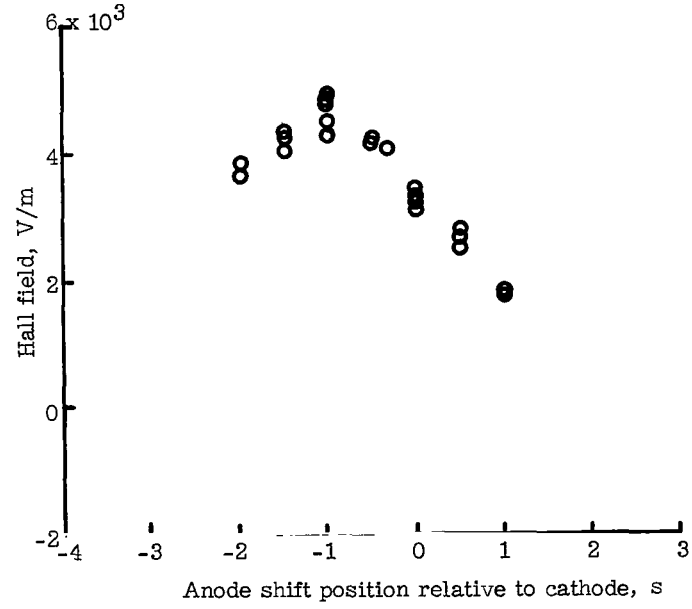

Figure 8.- Experimentally obtained variation of Hall field with electrode stagger taken from reference 16.

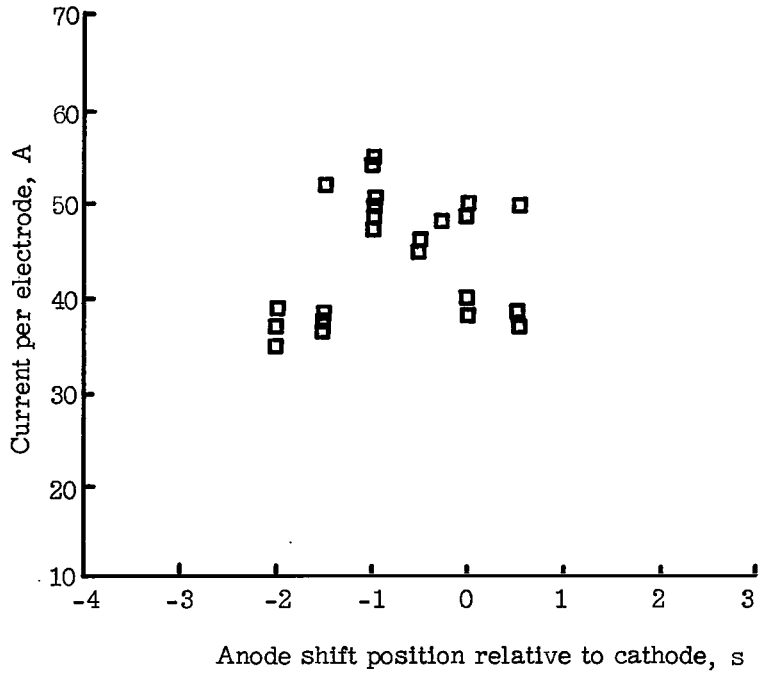

Figure 9.- Experimentally obtained variation of current per electrode as a function of electrode stagger taken from reference 16.

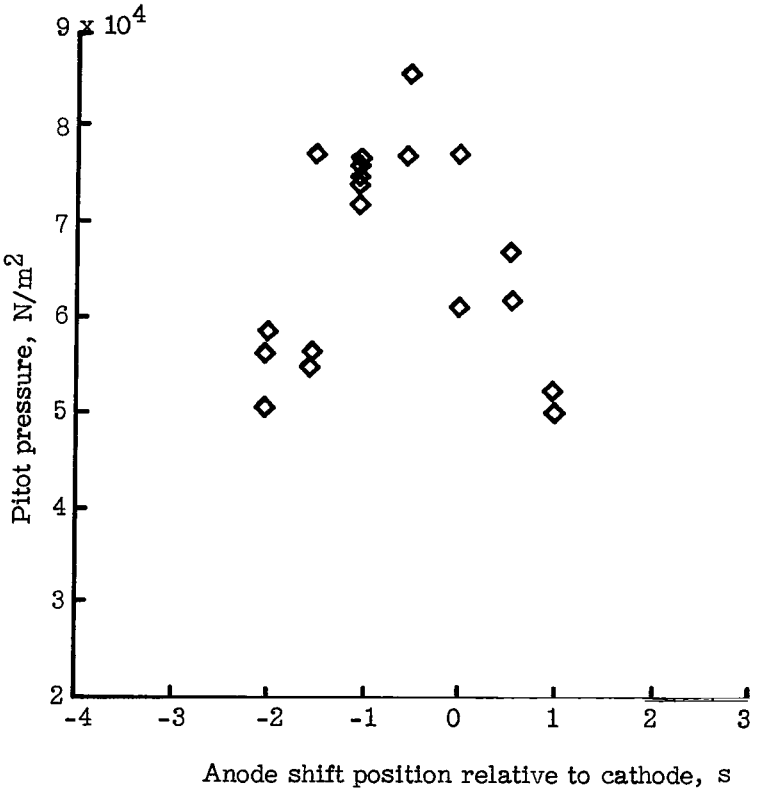

Figure 10.- Experimentally obtained pitot pressure as a function of electrode stagger taken from reference 16.

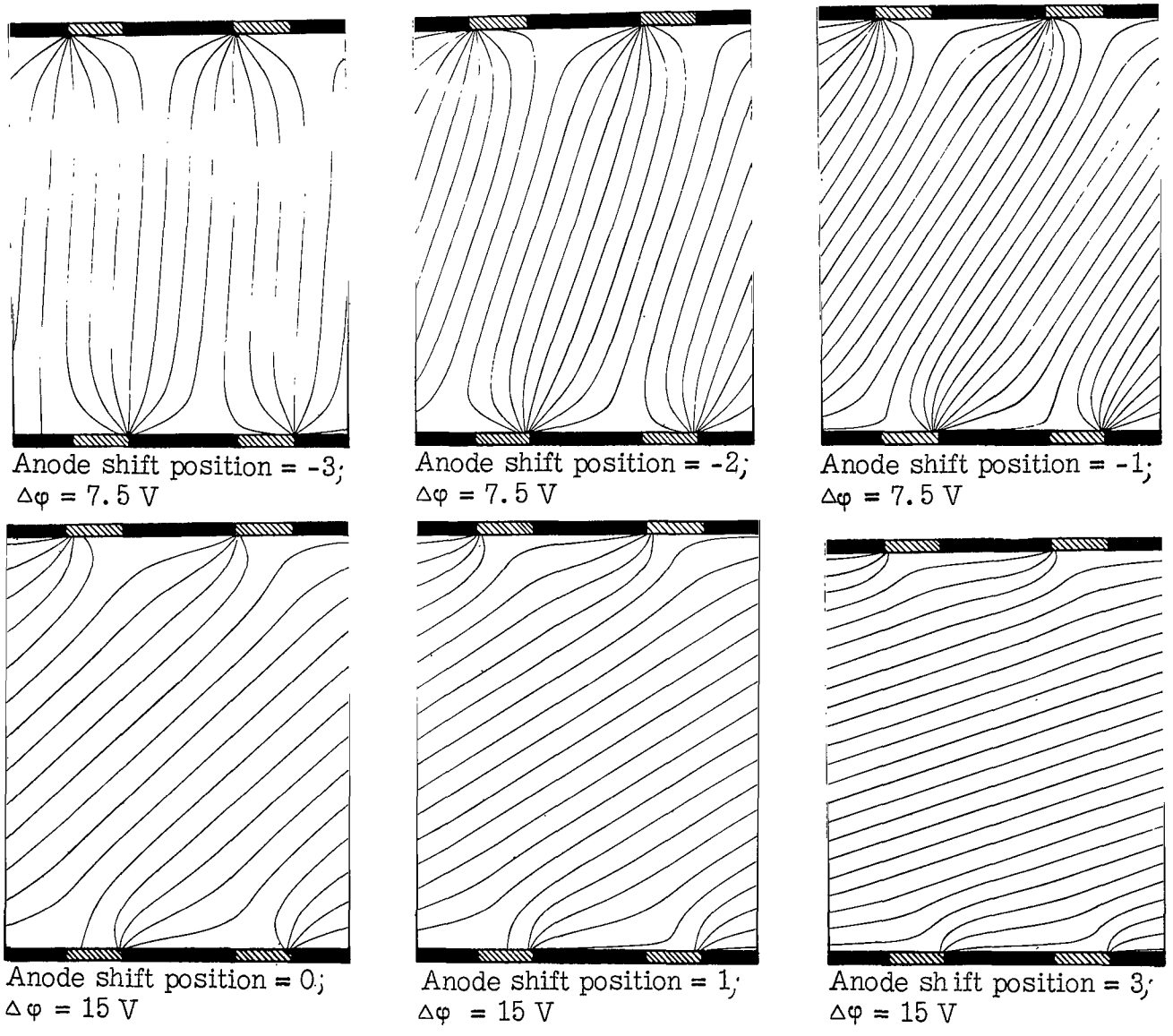

Figure 11.- Variation of equipotential lines as a function of electrode stagger. The top electrodes are the anodes and the flow direction is from left to right.

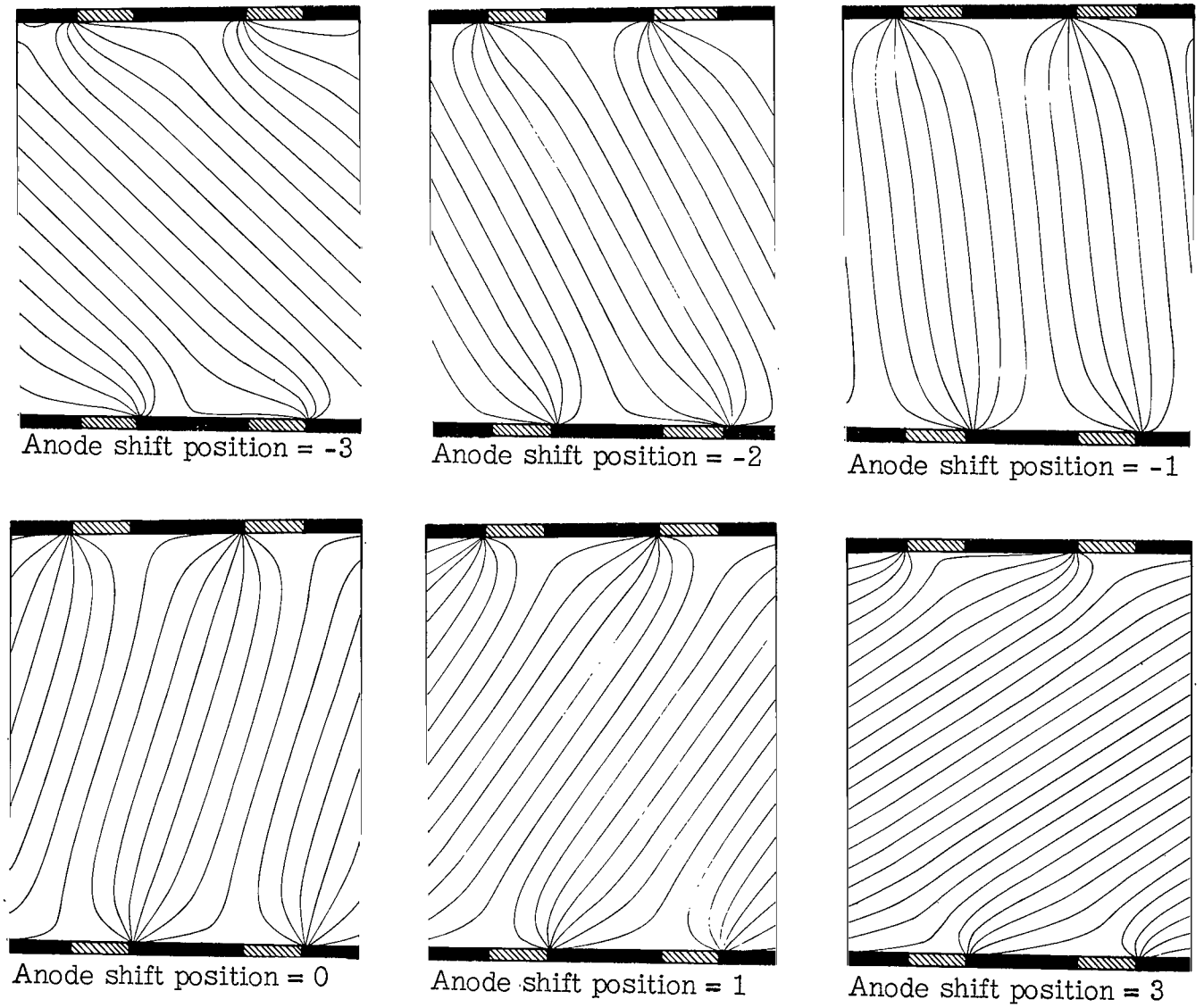

Figure 12.- Variation of lines of constant current flux as a function of electrode stagger. $\Delta\gamma$ = 300 A/m for all cases shown. The top electrodes are the anodes and the flow direction is from left to right.

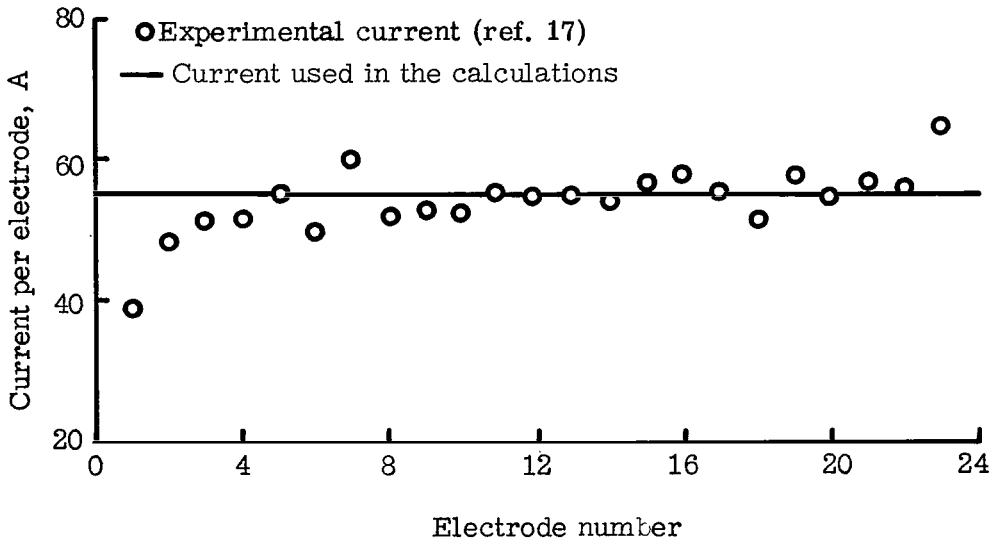

Figure 13.- Comparison of experimentally obtained electrode current with current used in calculations.

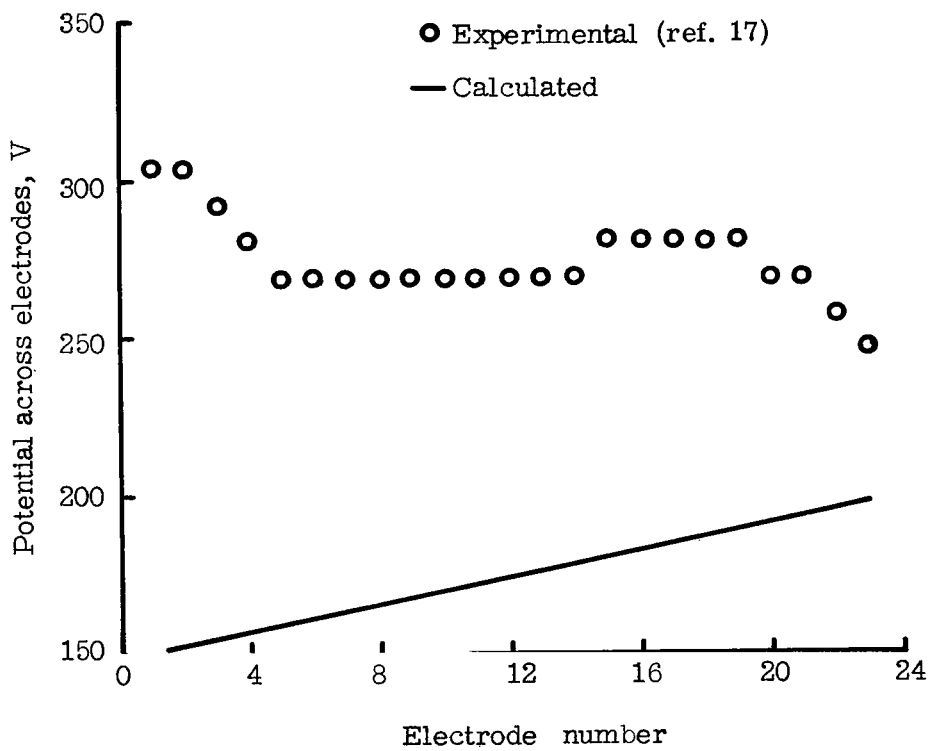

Figure 14.- Comparison of calculated potential applied between electrodes with experimental values.

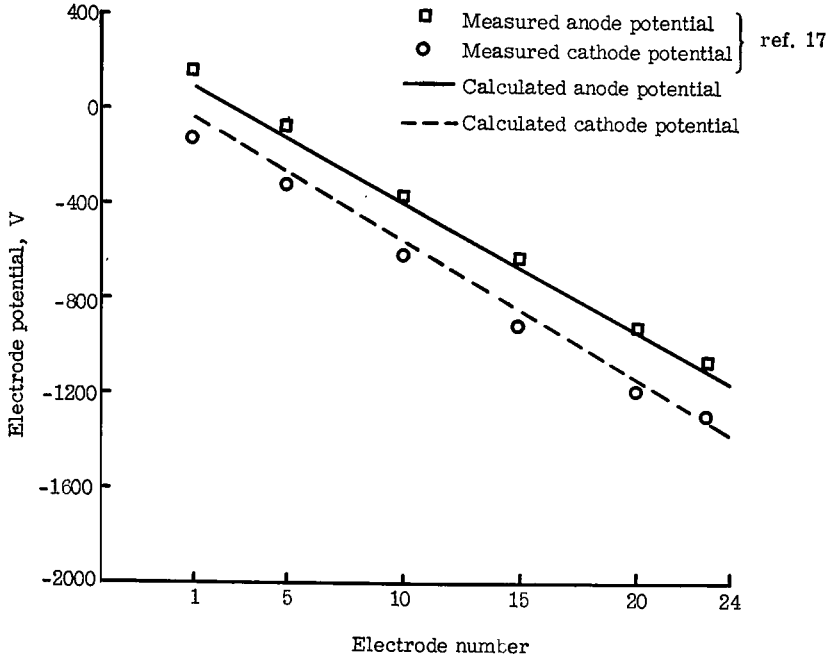

Figure 15.- Comparison of calculated electrode potential with experimental data from reference 17.

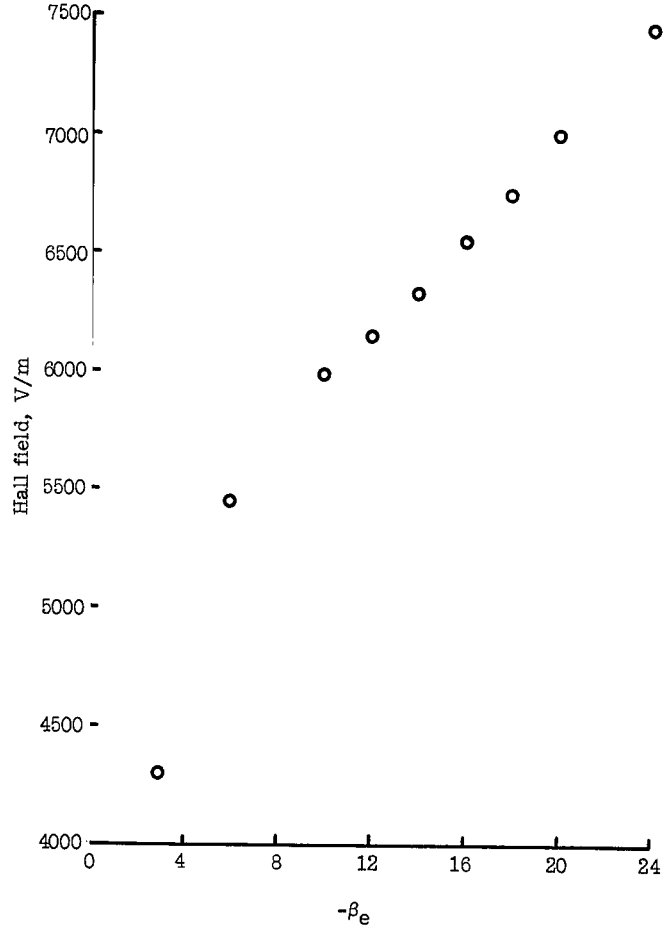

Figure 16.- Hall field as a function of the Hall parameter with B and σ constant.

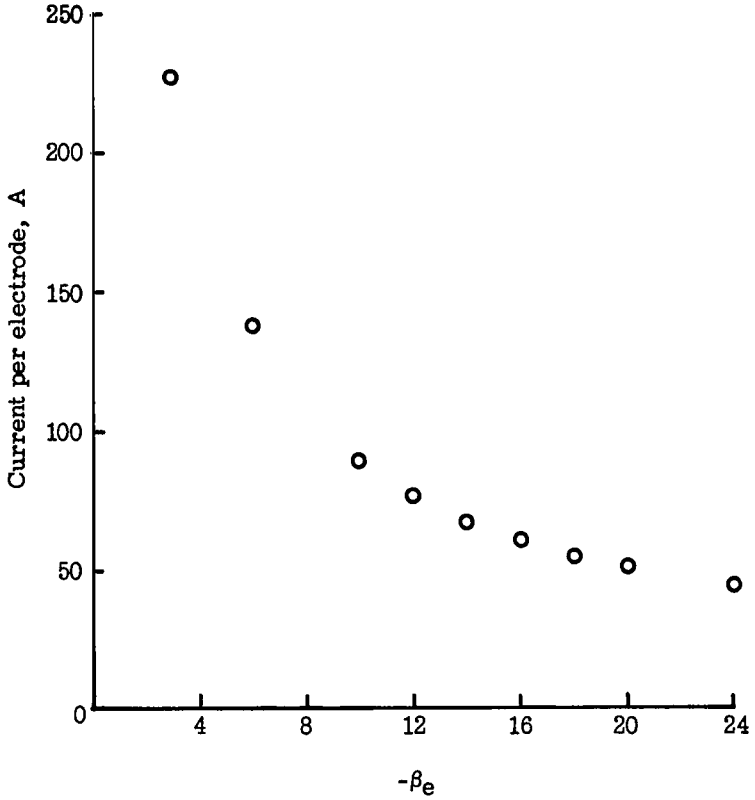

Figure 17.- Variation of electrode current with Hall parameter for B and σ constant.

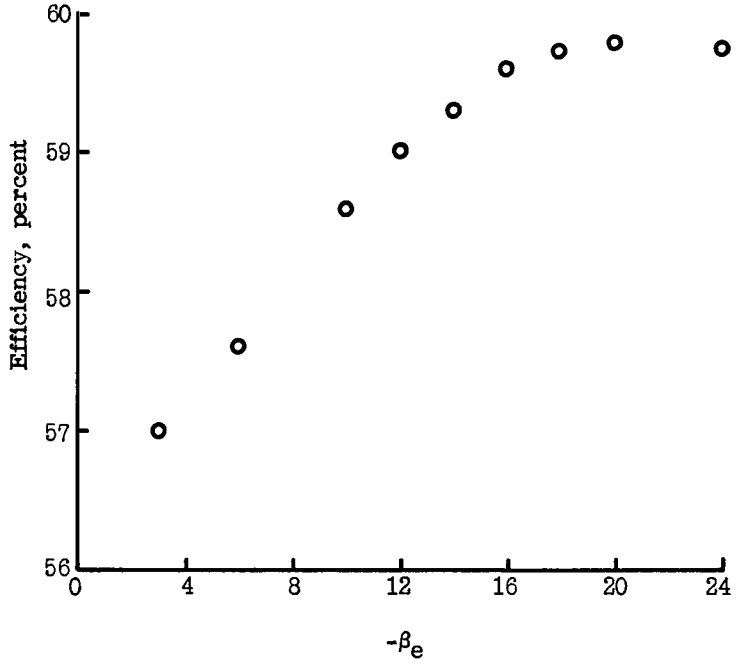

Figure 18.- Variation of efficiency with Hall parameter for B and σ constant.

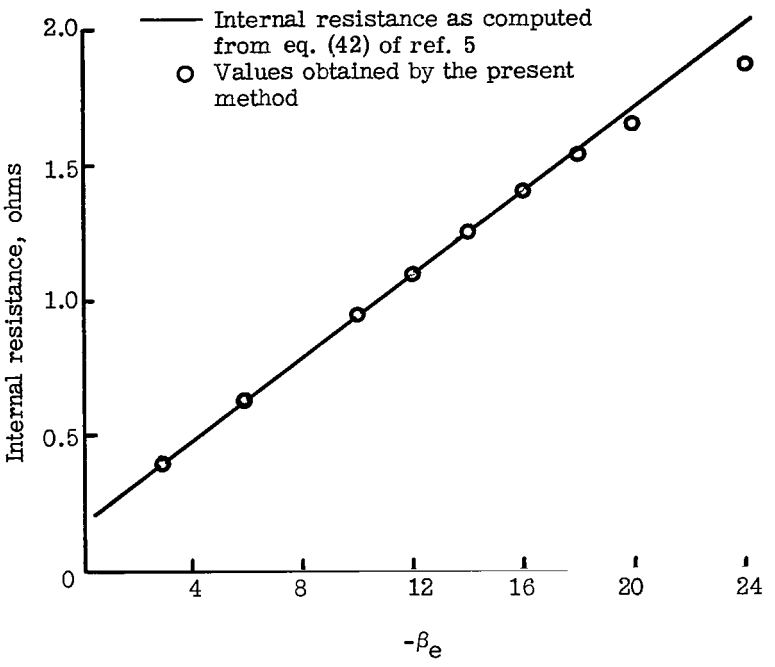

Figure 19.- Variation of internal resistance with Hall parameter for B and σ constant.

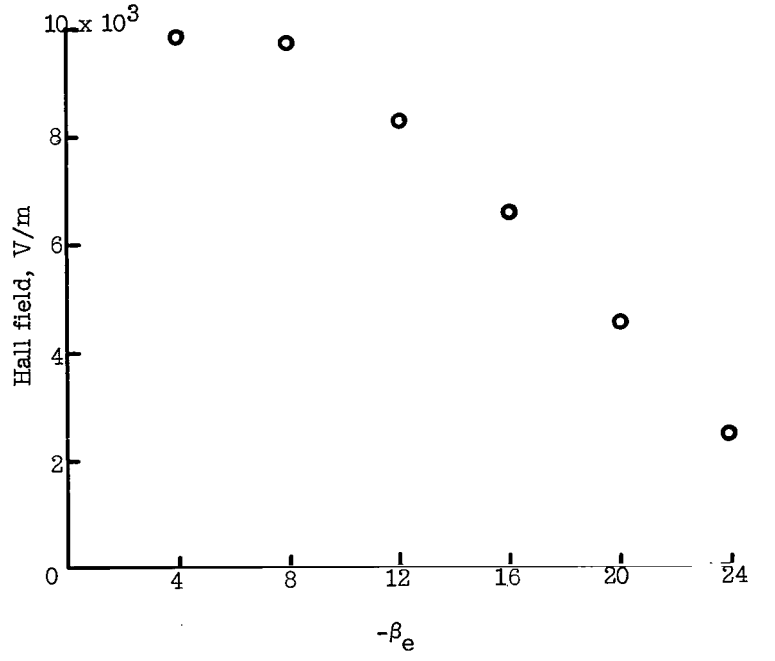

Figure 20.- Variation of Hall field with Hall parameter for β_e = 14B.

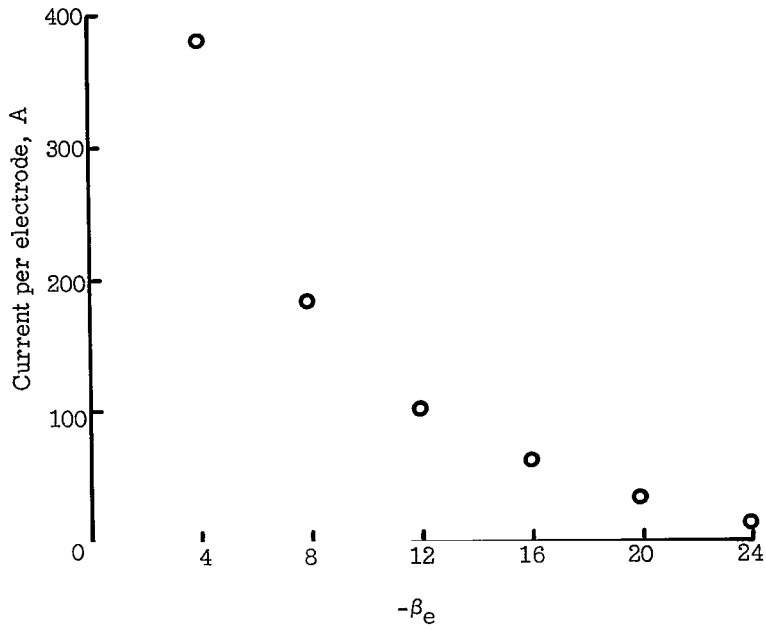

Figure 21.- Variation of electrode current with Hall parameter for β_e = 14B.

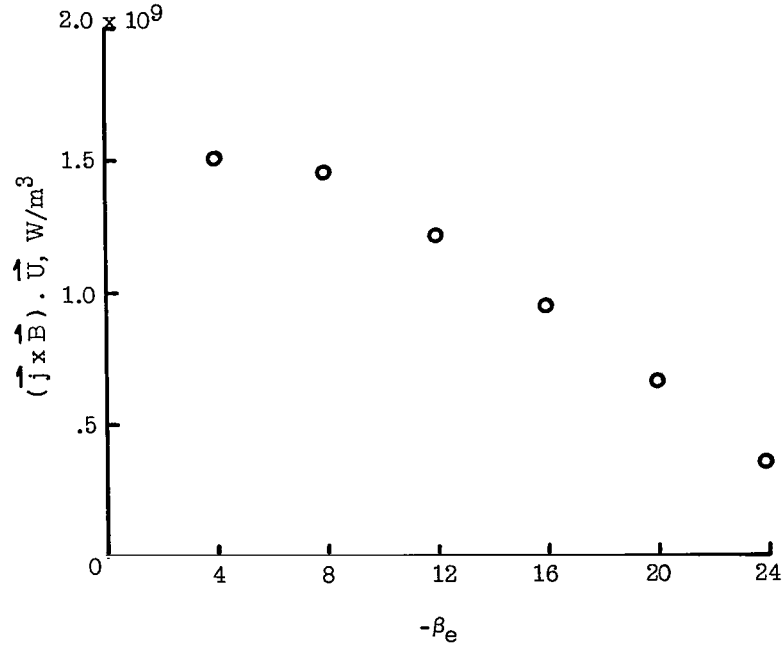

Figure 22.- Variation of work done with Hall parameter for β_e = 14B.

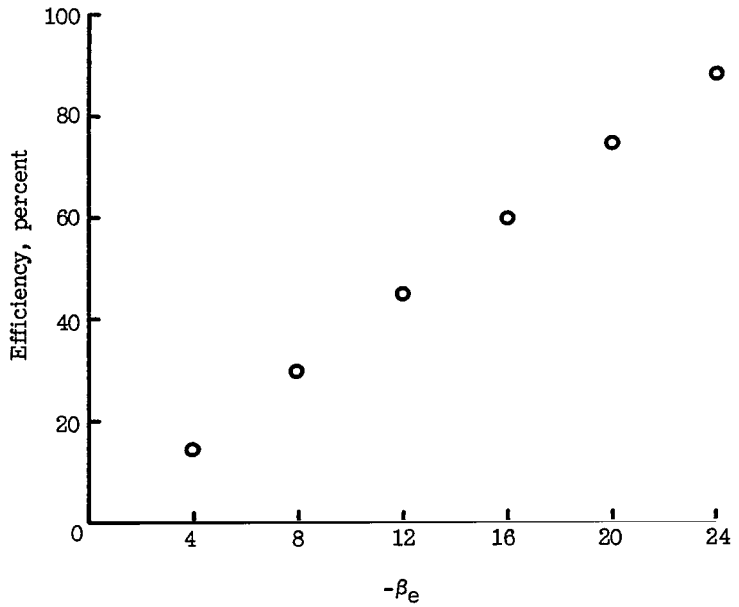

Figure 23.- Variation of efficiency with Hall parameter for β_e = 14B.

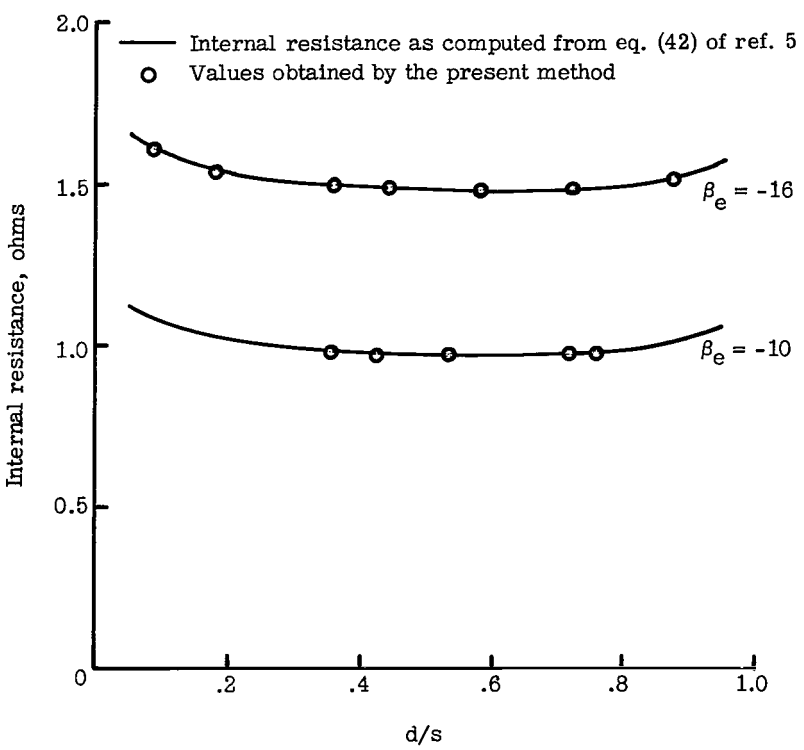

Figure 24.- Variation of internal resistance with d/s for β_e = -16 and β_e = -10.

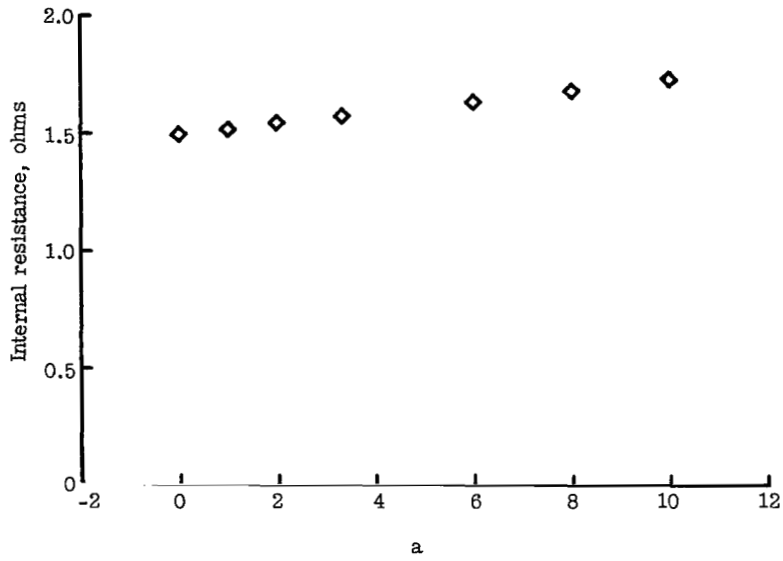

Figure 25.- Internal resistance as a function of velocity gradient.

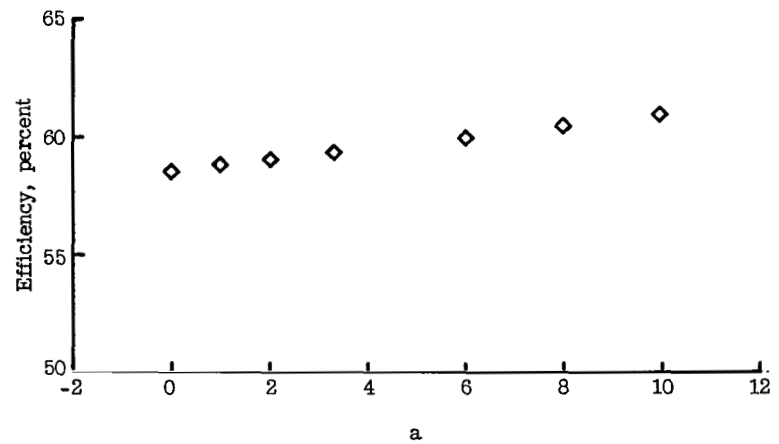

Figure 26.- Variation of efficiency with velocity gradient.

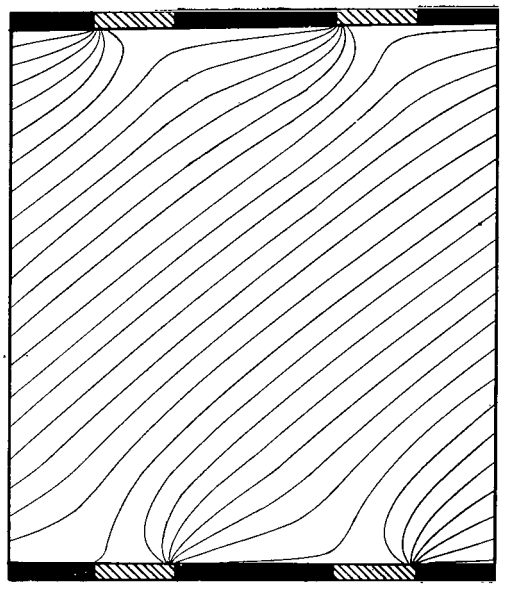

Equipotential lines;
a = 6; $\Delta\varphi$ = 10 V

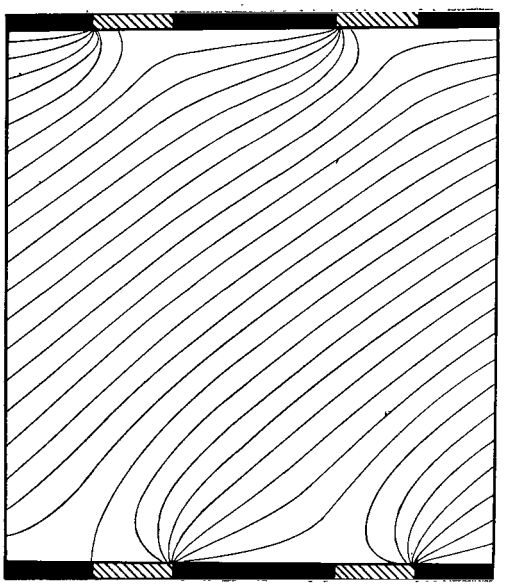

Equipotential lines;
a = 10; $\Delta\varphi$ = 10 V

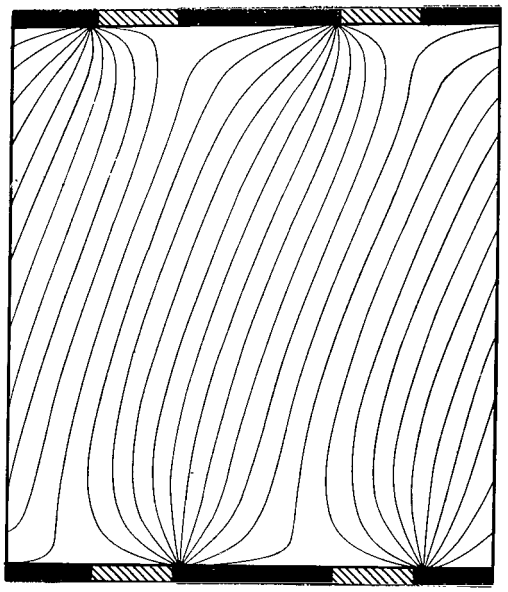

Lines of constant current flux;
a = 6; $\Delta\gamma$ = 200 A/m

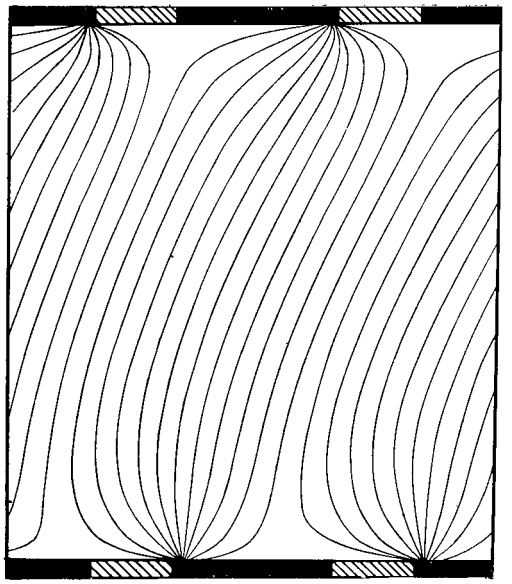

Lines of constant current flux;
a = 10; $\Delta\gamma$ = 200 A/m

Figure 27.- Variation of equipotential lines and current flux lines with a. The top electrodes are the anodes and the flow is from left to right.

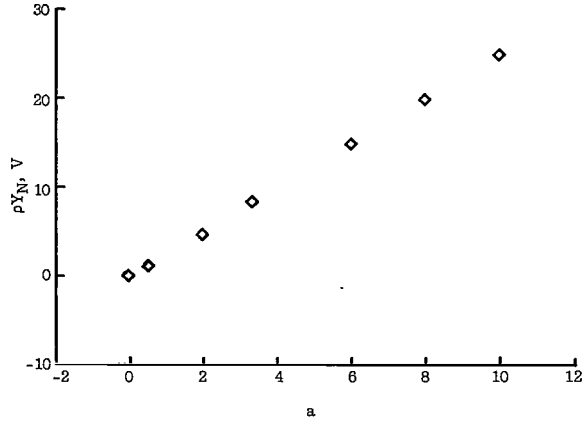

Figure 28.- Variation of ρY_N with a.

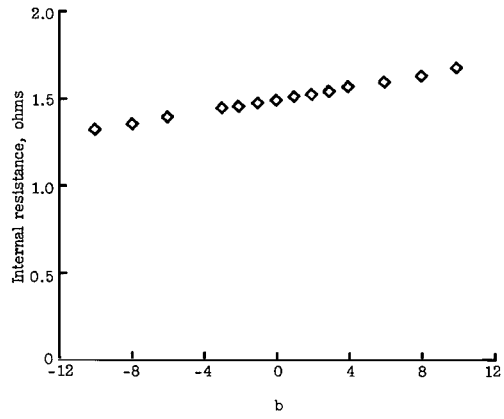

Figure 29.- Internal resistance as a function of b.

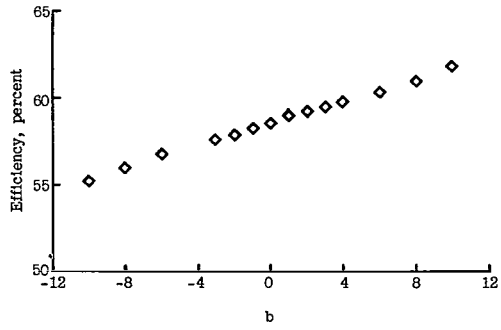

Figure 30.- Efficiency as a function of magnetic field gradient.

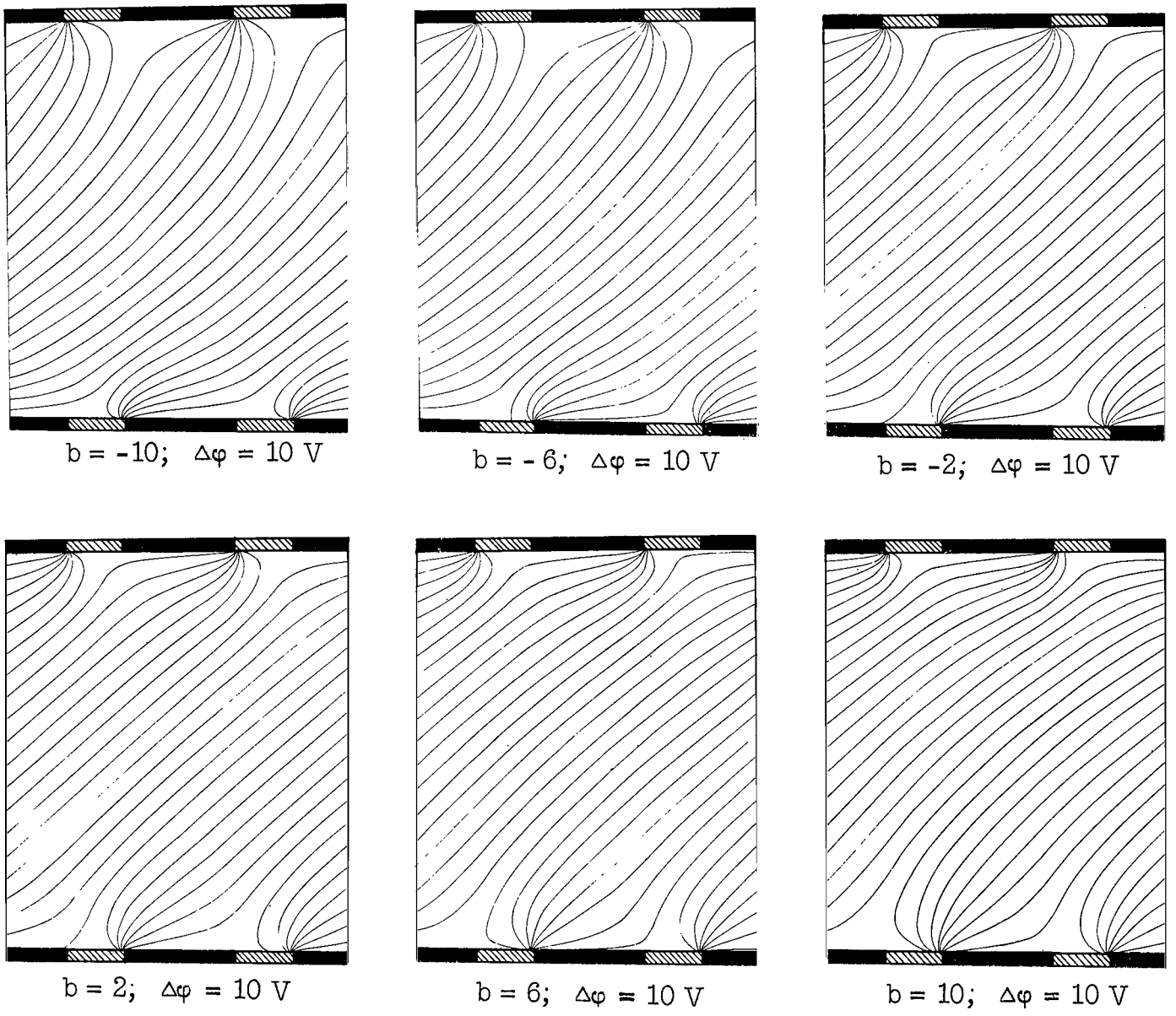

Figure 31.- Variation of equipotential lines with b. The top electrodes are the anodes and the flow direction is from left to right.

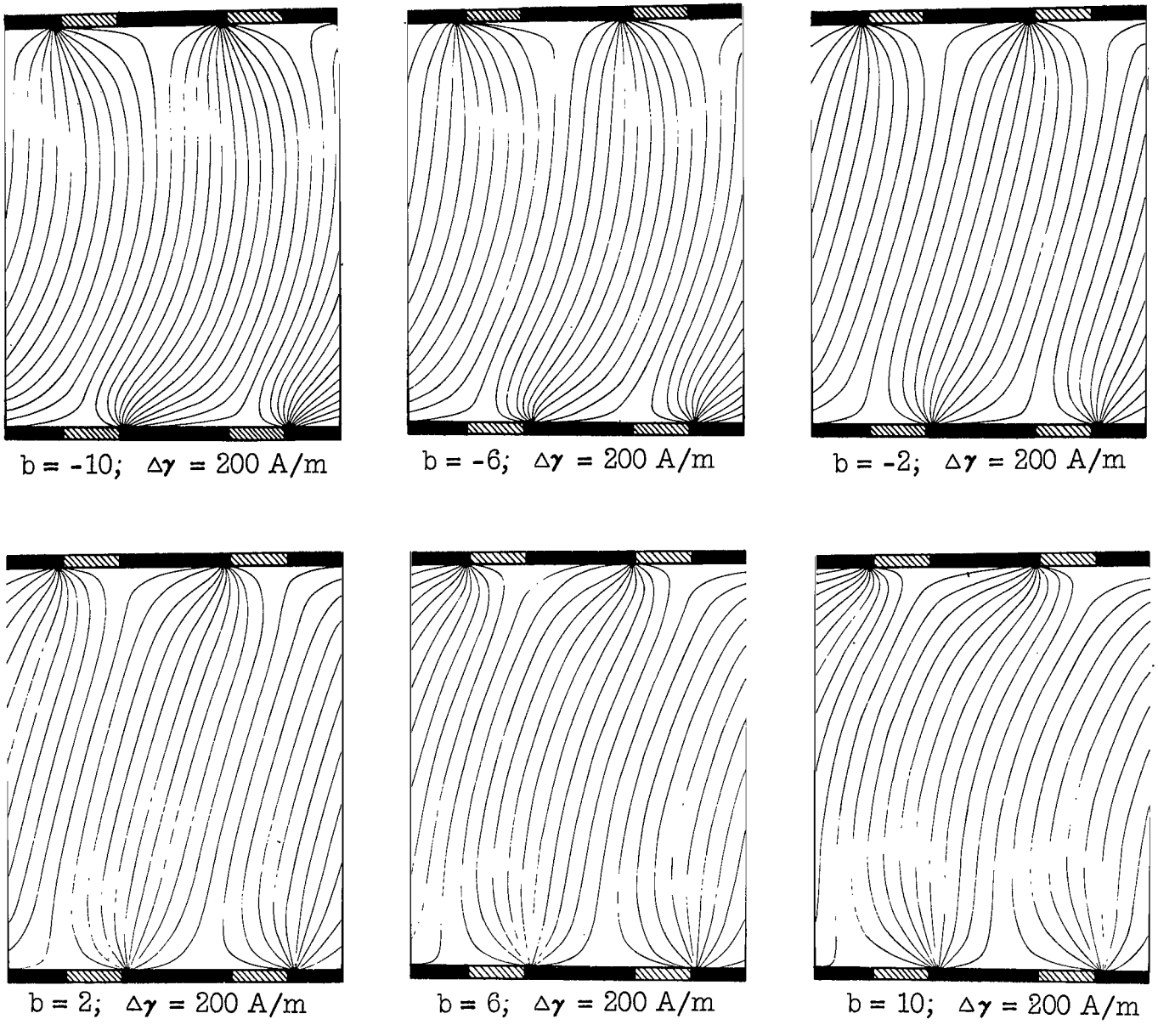

Figure 32.- Variation of constant current flux lines with b. The top electrodes are the anodes and the flow direction is from left to right.

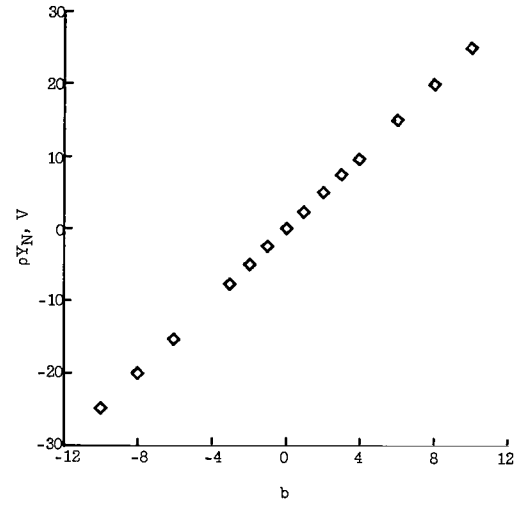

Figure 33.- Variation of ρY_N with b.

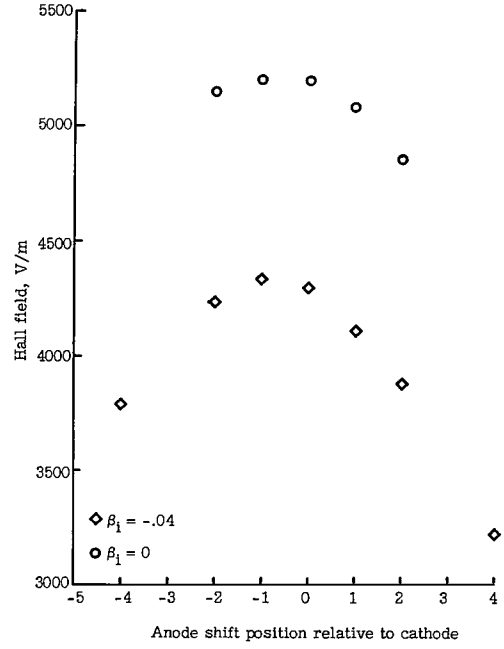

Figure 34.- Variation of Hall field with electrode stagger for the 6.35-cm-square accelerator.

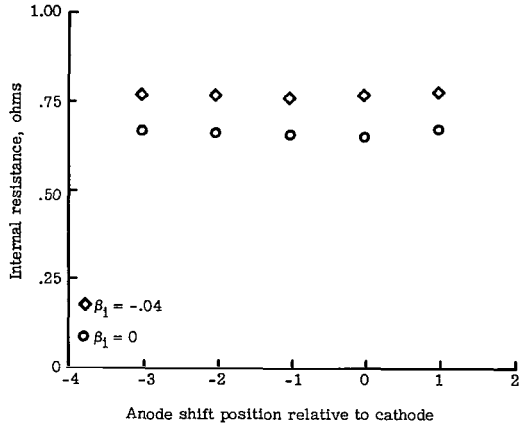

Figure 35.- Variation of internal resistance with electrode stagger for the 6.35-cm-square accelerator.

"The aeronautical and space activities of the United States shall be conducted so as to contribute . . . to the expansion of human knowledge of phenomena in the atmosphere and space. The Administration shall provide for the widest practicable and appropriate dissemination of information concerning its activities and the results thereof."

—NATIONAL AERONAUTICS AND SPACE ACT OF 1958

NASA SCIENTIFIC AND TECHNICAL PUBLICATIONS

TECHNICAL REPORTS: Scientific and technical information considered important, complete, and a lasting contribution to existing knowledge.

TECHNICAL NOTES: Information less broad in scope but nevertheless of importance as a contribution to existing knowledge.

TECHNICAL MEMORANDUMS: Information receiving limited distribution because of preliminary data, security classification, or other reasons.

CONTRACTOR REPORTS: Scientific and technical information generated under a NASA contract or grant and considered an important contribution to existing knowledge.

TECHNICAL TRANSLATIONS: Information published in a foreign language considered to merit NASA distribution in English.

SPECIAL PUBLICATIONS: Information derived from or of value to NASA activities. Publications include conference proceedings, monographs, data compilations, handbooks, sourcebooks, and special bibliographies.

TECHNOLOGY UTILIZATION PUBLICATIONS: Information on technology used by NASA that may be of particular interest in commercial and other non-aerospace applications. Publications include Tech Briefs, Technology Utilization Reports and Notes, and Technology Surveys.

Details on the availability of these publications may be obtained from:

SCIENTIFIC AND TECHNICAL INFORMATION DIVISION

NATIONAL AERONAUTICS AND SPACE ADMINISTRATION

Washington, D.C. 20546